

**POLITECNICO DI TORINO**

**Corso di Laurea Magistrale in Ingegneria Energetica e Nucleare**



Master of Science Thesis

**Effects of anode fuel recirculation on SOFCs fuelled  
with biogas**

**Tutors**

Prof. Ing. Massimo Santarelli

Prof. Dr. Anke Hagen (DTU Energy)

Prof. Andrea Lanzini

Hendrik Langnickel, MSc (DTU Energy)

**Master Student**  
Daniele Reschiotto

**Academic Year 2017-2018**



This thesis was realized at the Department of Energy Conversion and  
Storage,  
**Technical University of Denmark**



I would like to say thank you to Hendrik Langnickel and Anke Hagen for supervising me during these six months at DTU.  
In addition, many thanks to Ole Hansen, Henrik Henriksen and Martin Nielsen for helping out during problems in the laboratory.



# Abstract

Biogas is one of the most interesting renewable sources, composed by mainly by  $CH_4$ ,  $CO_2$  and  $N_2$ , with presence of other gasses, like for example  $H_2O$  and  $O_2$ , and impurities ( $H_2S$ , siloxanes, halogenous). In particular, landfill biogas, which has a low heating value, can be used in a solid oxide fuel cell (SOFC) in order to produce electricity, at higher efficiency with respect to internal combustion engine (ICE), plus the side product heat. A SOFC working with carbon-containing fuels needs a reforming agent, such as steam, carbon dioxide or oxygen, in order to avoid carbon deposition, which leads to a fast degradation of the cell. Another option to avoid carbon formation is to substitute the reforming agent by applying the recirculation of the anode off-gases again at the cell inlet. The current study investigates the recirculation of the anode exhaust gas to avoid carbon formation in a SOFC fuelled with biogas. Therefore, a theoretical simulation study has been carried out firstly, with the aim of understanding the general relationship between the recirculation ratio (RR), which means the amount of anode off-gases recirculated, and the carbon activity and so to identify the boundary conditions. In the second part laboratory tests were carried out. For each simulation and test a planar cell of  $16\text{ cm}^2$  operating at  $750^\circ\text{C}$  has been employed, with different types of biogas: pre-mixed landfill (low methane content), pre-mixed wastewater (high methane content) and real biogas. The pre-mixed biogas were mixed directly with mass flow controller in the test rig and no impurities were considered. In the case of real landfill biogas a pre-cleaning was done to remove undesired compounds. For the experimental study, two scenarios were tested. In the first one, the expected anode exhaust gas according to the simulations was pre-mixed via mass flow controllers. In the second study, the real anode exhaust gas was recirculated using a pump. Cell performance and degradation were analyzed considering different RR, comparing not only the results obtained from simulations and tests but also the differences with respect to the biogas composition. Simulations and experiments show a decrease of carbon activity proportional to the RR, both for landfill and wastewater, while a decrement of degradation rate and a rise of electric efficiency (from 2 to 5 percentage points) in inverse proportion to RR are observed.



# Contents

<b>1</b>	<b>Introduction</b>	<b>1</b>
<b>2</b>	<b>Fundamentals</b>	<b>3</b>
2.1	Fuel Cell . . . . .	3
2.1.1	Solid Oxide Fuel Cell . . . . .	3
2.1.2	Carbon deposition . . . . .	11
2.1.3	Fuel recirculation: advantages and principal aim . . . . .	13
2.1.4	Power and efficiency of a fuel cell . . . . .	15
2.2	Biogas . . . . .	16
2.2.1	Contaminants . . . . .	16
2.2.2	Type of biogas analyzed . . . . .	17
<b>3</b>	<b>Theoretical study</b>	<b>19</b>
3.1	Simulation set up . . . . .	19
3.1.1	Simulation description . . . . .	19
3.1.2	Biogas anode fuel recycling study: simulation . . . . .	27
3.2	Results of simulations study . . . . .	28
3.2.1	Landfill: pre-mixed biogas . . . . .	28
3.2.2	Waste water: pre-mixed biogas . . . . .	33
<b>4</b>	<b>Experimental study</b>	<b>37</b>
4.1	Experimental set up . . . . .	37
4.1.1	Description of the test rig . . . . .	38
4.1.2	Cell start up and fingerprint . . . . .	42
4.1.3	Impedance spectroscopy: definition and characteristics . . . . .	43
4.1.4	Biogas anode fuel recycling study: test . . . . .	46
4.2	Results of tests study . . . . .	47
4.2.1	Landfill: pre-mixed biogas . . . . .	48
4.2.2	Waste Water: pre-mixed biogas . . . . .	55
4.2.3	Recirculation using pump: pre-mixed and real biogas . . . . .	61

<b>5 Comparison</b>	<b>73</b>
5.1 Evaluation of differences in cell performance . . . . .	73
5.2 Evaluation of the degradation rate for all experiments . . . . .	75
<b>6 Conclusions</b>	<b>77</b>
<b>7 Future outlook</b>	<b>79</b>
<b>Bibliography</b>	<b>81</b>

# List of Figures

1.1	Landfill biogas anaerobic digestion from waste . . . . .	2
2.1	Scheme of a SOFC . . . . .	4
2.2	Structure of an anode supported SOFC . . . . .	6
2.3	Polarization curve of a generic fuel Cell . . . . .	8
2.4	Carbon deposition boundaries . . . . .	12
2.5	Scheme of the recirculation implementation . . . . .	13
2.6	Volumetric flows with and without recirculation . . . . .	14
2.7	Different biogas composition with respect to NG . . . . .	16
3.1	Scheme of simulation . . . . .	20
3.2	Scheme of the virtual SOFC . . . . .	22
3.3	Carbon activity behavior with current and 50% of recirculation	24
3.4	Landfill: carbon activity behaviour depending on RR with different FU . . . . .	25
3.5	Animal Waste: carbon activity behaviour depending on RR with different FU . . . . .	26
3.6	Waste Water: carbon activity behaviour depending on RR with different FU . . . . .	27
3.7	Landfill: molar flows along the cell, final step FU = 60% . . .	29
3.8	Landfill: carbon activity with respect to RR, FU = 60% . . .	32
3.9	Landfill: carbon activity with respect to RR, FU = 80% . . .	32
3.10	Waste Water: molar flows along the cell, final step FU = 80%	34
3.11	Waste water: carbon activity with respect to RR, FU = 60% .	36
3.12	Waste water: carbon activity with respect to RR, FU = 80% .	36
4.1	Rig 5 set up, with exhaust recycling, biogas and particle filters	38
4.2	Image of the cathode side of the cell after test, including the gold sealing . . . . .	39
4.3	Cell house section . . . . .	40
4.4	Anode part (left) and cathode part (right) of the cell house . .	41

4.5	Nyquist plot . . . . .	43
4.6	Bode plot . . . . .	44
4.7	ASR percentage increment in 1000 h with extra $CO_2$ . . . . .	49
4.8	i-U curves from test 1 and test 2 . . . . .	52
4.9	Experimental data from test 1 and test 2 . . . . .	53
4.10	Voltage evolution from test 1 and test 2 . . . . .	54
4.11	i-U curves from test 3 and test 4 . . . . .	58
4.12	Experimental data from test 3 and test 4 . . . . .	59
4.13	Voltage evolution from test 3 and test 4 . . . . .	60
4.14	Voltage over time, pre-mixed landfill RR = 50%, 600 h . . . . .	63
4.15	Experimental data from test 5, test 6 and test 7 . . . . .	66
4.16	i-U curves from test 5, test 6 and test 7 . . . . .	67
4.17	Voltage evolution from test 5, test 6 and test 7 . . . . .	68
4.18	Experimental data from test 8 . . . . .	70
4.19	Voltage evolution and i-U curve from test 8 . . . . .	71
5.1	Voltage comparison between simulations and tests . . . . .	74
5.2	Efficiency and degradation rate summary . . . . .	76

# List of Tables

1.1	Biogas production for heat and electricity in the European Union	1
2.1	Composition of the three biogas . . . . .	17
3.1	Table of species . . . . .	20
3.2	Simulation parameters . . . . .	21
3.3	Input parameters value . . . . .	21
3.4	FU-current density . . . . .	25
3.5	Pre-mixed biogas simulations overview . . . . .	27
3.6	Pre-mixed landfill simulations results in terms of voltage and efficiency, different FU . . . . .	28
3.7	Pre-mixed wastewater simulations results in terms of voltage and efficiency, different FU . . . . .	33
4.1	SoA anode supported cell materials . . . . .	39
4.2	Basic circuit elements impedance . . . . .	44
4.3	Anode polarization processes and key factors with respect to frequency in impedance spectra for a SOFC cell consisting of Ni-YSZ . . . . .	45
4.4	Pre-mixed biogas experiments overview with pre-mixed recirculation . . . . .	46
4.5	Pre-mixed and real biogas experiments using pump to recirculate	47
4.6	Landfill: experiments with pre-mixed recirculation . . . . .	48
4.7	Test 0: average voltage, power and efficiency without recirculation . . . . .	48
4.8	Test 1: average voltage, power and efficiency with recirculation of 50% . . . . .	50
4.9	Test 2: average voltage, power and efficiency with recirculation of 30% . . . . .	51
4.10	Waste water: experiments without pump . . . . .	55

4.11	Test 3: average voltage, power and efficiency with recirculation of 50% . . . . .	56
4.12	Test 4: average voltage, power and efficiency with recirculation of 30% . . . . .	57
4.13	Landfill: experiments with pump . . . . .	61
4.14	Test 5: average voltage, power and efficiency with recirculation of 50% . . . . .	62
4.15	Test 6: average voltage, power and efficiency with recirculation of 30% . . . . .	64
4.16	Test 7: average voltage, power and efficiency with recirculation of 10% . . . . .	65
4.17	Test 8: average voltage, power and efficiency with recirculation of 30% . . . . .	70

# Chapter 1

## Introduction

Biogas production has been increased of approximately 78% in the last few years, as reported by Achinas et al. [1] and Scarlat et al. [2], due to the fact that it is an interesting source, especially for electrochemical conversion devices like fuel cells, and it allows reducing environmental impact, as claimed by Lunghi et al. [3]. The increase of biogas production in Europe (in toe<sup>1</sup>) is reported in table 1.1.

Calendar year	Total (toe)	Calendar year	Total (toe)
2009	7934	2013	13491
2010	8504	2014	13770
2011	10341	2015	14000
2012	12044	2016	14120*

\*estimated

Table 1.1: Biogas production for heat and electricity in the European Union (from [1])

The main components of biogas are methane, carbon dioxide and nitrogen, with also the presence of some other gases, such as oxygen and water/steam, and impurities (sulfur, siloxanes, halogenous). The composition strongly depends on the biogas source, which can be waste, sewage, animal residuals, agriculture residuals, sludge, etc. In particular, landfill biogas is coming from anaerobic digestion of municipal waste (fig. 1.1) and its characteristics are low content of methane, while very high content of nitrogen. These properties make it perfectly suitable to use in a solid oxide fuel cell

---

<sup>1</sup>Tonne of oil equivalent.

(SOFC), as already proved by Hagen et al. [4, 5] and Meng et al. [6], device able to produce electricity at high efficiency and heat as a side product.

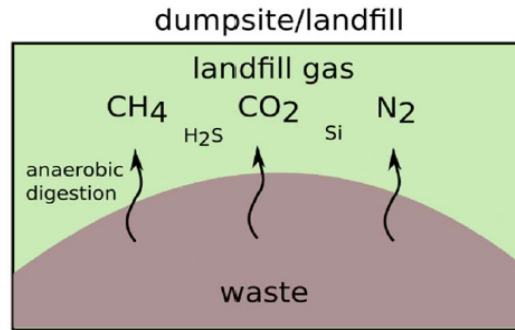


**Figure 1.1: Landfill biogas anaerobic digestion from waste (from [7])**

Carbon-containing fuels are problematic for SOFCs, since particles of carbon can deposit at the anode, leading to the break down of the cell. In order to avoid it, a reforming agent is added to the fuel, choosing among  $\text{CO}_2$ ,  $\text{H}_2\text{O}$  and pure  $\text{O}_2$ : this means that an external supply is always needed to run the cell in safe conditions.

The aim of this work is to prove that external supply of reforming agent is not needed anymore to avoid carbon deposition if recirculation of the anode off-gases is applied to the cell (except for the start up and shut down) and moreover a gain in efficiency should be observed (as explained by Dietrich et al. [8]). Initially, simulations using Gibbs free energy minimization for the calculation of the equilibrium (as done in [9–12]) and carbon activity ( $a_c$ ) have been implemented, to generally understand the relationship between  $a_c$  and recirculation ratio (RR), which is the percentage of anode off-gases recirculated. The second part has been dedicated to experimental tests at cell level, in order to prove what has been discovered in the simulation part. Both have been carried out using different types of pre-mixed biogas (landfill, waste water) and real landfill biogas. Carbon activity and efficiency are considered in order to evaluate the performance of the system, while degradation rate of voltage and area of specific resistance (ASR) are used to understand the general degradation of the cell.

It has been demonstrated, both from simulations and laboratory tests, that fuel recirculation is able to face the problem of carbon activity and, furthermore, an increment of the cell electric efficiency is observed, which can arrive at 5-6%.

# Chapter 2

## Fundamentals

### 2.1 Fuel Cell

Fuel cells are galvanic cells able to convert hydrogen and oxygen into steam, with the production of electricity and heat at high efficiency, compared to internal combustion engine (ICE), and low pollutant emissions. This is due to electrochemical reactions among molecules, avoiding direct combustion, so the produced heat is lower and, as a consequence, more fuel is converted into electricity. In addition, they are silent, allowing placing them everywhere. The general reaction involved inside the cell, considering pure  $H_2$  fed, is:



Fuel cells are divided into three groups, depending on their operation temperature:

- Low temperature fuel cells (  $50^\circ < T < 150^\circ\text{C}$ );
- Medium temperature fuel cells (  $200^\circ < T < 250^\circ\text{C}$ );
- High temperature fuel cells (  $600^\circ < T < 1000^\circ\text{C}$ );

The different operating temperature is related to the electrolyte layer and influences the kinetic and thermodynamic of the processes, as can be seen more in details in manuals (i.e [13]). In this work a solid oxide fuel cell is used, so the description will mainly regard this type of fuel cell.

#### 2.1.1 Solid Oxide Fuel Cell

As every type of fuel cell, SOFC takes the name from the used electrolyte, which is, in this case, a thin layer of oxides of transition metals or rare

earth metal (so, ceramics). The operating temperature is between  $500^{\circ}\text{C}$  and  $1000^{\circ}\text{C}$ . An example of a SOFC type fuel cell is represented in figure 2.1, from [14]

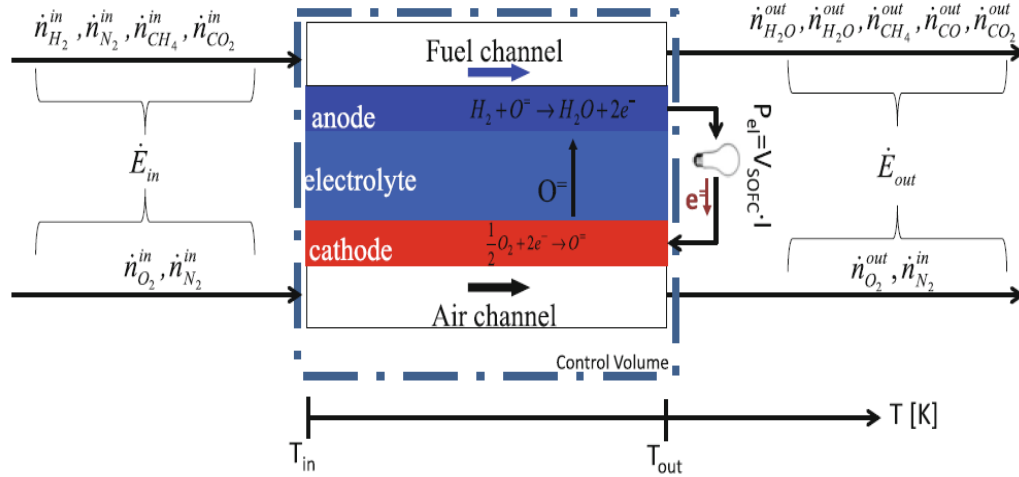


Figure 2.1: Scheme of a SOFC

Working at high temperature has some advantages [15], with respect to low temperature fuel cell (such as PEMFC or Alkaline):

- a very good kinetic of electrochemical reactions and ionic conductivity, which means having a higher efficiency;
- fuel flexibility, which allows using not only hydrogen ( $H_2$ ), but also hydrocarbons, alcohols, biogas, syngas. etc.;
- no precious catalyst is needed, so the most used one is nickel(Ni), which is not very expensive;
- availability of heat at high temperature, with the possibility to generate hybrid configuration having a really high efficiency ([16]).

On the other hand, these temperatures have some disadvantages [13], such as:

- materials of cells and auxiliaries are expensive;
- the switch on/off time is very long (hours);
- number of thermal cycles is limited.

A solid oxide fuel cell is made by three different layers, called anode, electrolyte and cathode (fig. 2.1). At the anode, the oxidation reaction takes place, in which the fuel reacts with the ions coming from the electrolyte, forming steam and delivering electrons:



The electrolyte is a material sufficiently thin to allow  $O^{2-}$  to pass, but it has to block both electrons, to avoid short circuits, and molecules, otherwise combustion takes place. Finally, at the cathode, the reduction reaction takes place, where ions are formed due to the oxygen present in the air.



The state of the art (SoA) SOFC is made by the following materials:

**Anode** : The anode has to be porous in order to allow molecules transportation. Moreover, it needs the so called three phase boundary (TPB), which means having a catalyst, an ionic phase and an electronic phase: this is the reason a porous cermet (mix of ceramic-metallic) is used. The state of the art (SoA) is Yttria stabilised zirconia (YSZ) as a ceramic material and nickel as a catalyst. The first one is a mixture of two ceramic powder, zirconia ( $ZrO_2$ ) and Yttria ( $Y_2O_3$ ). A pathway of Ni and YSZ has to be created to have a good conductivity. Usually, the structure is graduated in porosity ( $\epsilon$ ), having a higher  $\epsilon$  near the fuel entrance and lower at the bound with the electrolyte, as illustrated in figure 2.2.

**Electrolyte** : As well as the anode layer, the electrolyte is usually made by the same mixture of ceramic powder:  $ZrO_2$  and  $Y_2O_3$ . Vacancies of oxygen in the lattice generate a good condition of mobility of  $O^{2-}$  ions, migrating from the cathode to the anode. The resistivity of YSZ ( $\rho_{YSZ}$ ) is quite high for low temperature, but it decreases working above  $700^\circ\text{C}$  so: this is the reason why operating temperatures of SOFCs are high. The thickness of the electrolyte has to be as small as possible, since it influences the ohmic losses (described in the next part), but not too much, in order to avoid short circuits.

**Cathode** : The cathode has to be a mixed ionic-electronic conductor. The SoA is made by lanthanum-strontium-manganese ( $La_{1-x}Sr_xMnO_3$ ), which is

represented by the acronym LSM. LSM has a perovskite structure, which assures good mechanical and thermal properties. LSM is not the only material, but in this brief description, the SoA is considered.

Regarding the structure of the SOFC, the most used is the anode supported one, in which the anode has both electrochemical and structural function. A microscopy image of a SOFC cell is shown in figure 2.2.

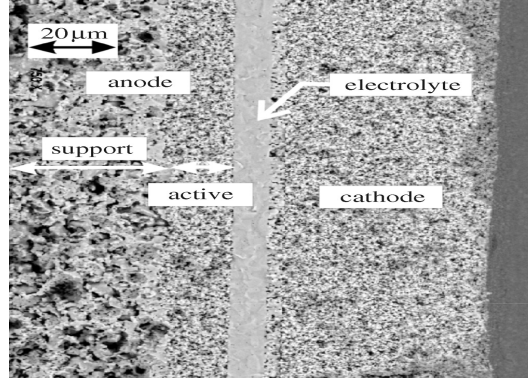
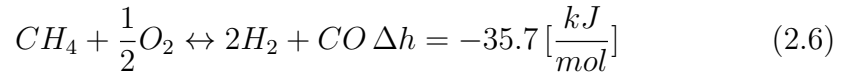
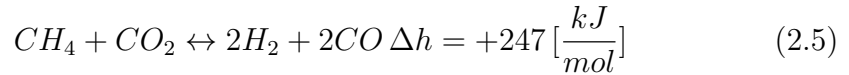
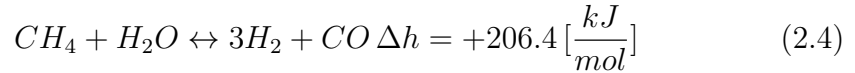


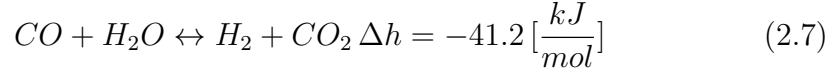
**Figure 2.2: Structure of an anode supported SOFC**

Owing to the fact that SOFCs work at high temperature and due to the presence of nickel at the anode, which works as a catalyst, internal reforming of hydrogen-rich fuels is happening, allowing feeding the cell with different types of fuel, such as hydrocarbons (i.e. methane), alcohols, etc. As a consequence, other reactions take place between anode and electrolyte. Considering methane, in equilibrium conditions, what in principle should happen inside the cell is the decomposition of methane due to  $H_2O$ ,  $CO_2$  or pure  $O_2$ , respectively called methane steam reforming (MSR, 2.4), dry reforming (DR, 2.5) and partial oxidation (PO, 2.6), into pure hydrogen and carbon monoxide:



The first two are endothermic reactions, so heat is produced and helps to maintain the high temperature of the cell, while the third one is slightly exothermic, so it absorbs heat, helping to regulate the temperature. Depending on the internal conditions, there are also other possible reactions, not of

interest for this work, but available in manuals as well as the previous one (see [13]). Moreover, the presence of  $H_2O$  and  $CO$  at the anode side, results in the so called water gas shift (WGS, 2.7) reaction, slightly exothermic as well as 2.6:



In order to calculate the equilibrium for more than one reaction, the Gibbs free energy is needed and, more specifically, it has to be minimized. The total Gibbs free energy is defined as follow:

$$G_{system} = \sum n_j \bar{G}_j \quad (2.8)$$

where  $\bar{G}_j$  is the molar Gibbs free energy and  $n_j$  represents the moles of the  $j$  species. The molar Gibbs free energy is defined as the sum of the standard Gibbs free energy and the activity, which is equal to the pressure using the assumption of working with ideal gases:

$$\bar{G}_j = G_j^0 + RT \ln(a_j) \quad (2.9)$$

and  $G_j^0$  comes from the difference between the enthalpy and the product of temperature and entropy of the species, as follow:

$$G_j^0 = H_j^0 - T \cdot S_j^0 \quad (2.10)$$

In other works, such as Joon et al. [9], also the condensed part is considered, where the activity  $a_j$  assumes a unitary value, but this is not the case since it is not expected condensation. Further detailed information about Gibbs free energy can be found in the literature ([13], [15]).

Working under a certain amount of current, the situation changes, since electrons start moving and ions of  $O^{2-}$  are going from the cathode to the anode side.

The trend of cell voltage can be evaluated looking at the polarization curve ( figure 2.3):

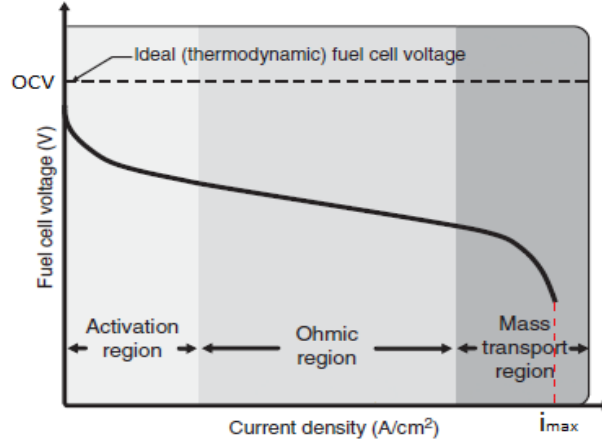


**Figure 2.3: Polarization curve of a generic fuel Cell**

The maximum value of the voltage, which is the point on the left, is called open circuit voltage (OCV) and it represents the voltage of the cell in equilibrium conditions, so if there is no current flowing. The OCV is defined by the Nernst equation:

$$OCV = Emf = \frac{-\Delta\bar{g}_{Re}(p, T)}{z_e F} \quad (2.11)$$

where  $Emf$  is the other way to call the OCV, and it means electromotive force,  $z_e$  is the number of electrons involved in the reaction, which depends on the type of fuel entering in the cell,  $F$  is the Faraday's constant, and its value is 96485 [s A/mol]. Finally  $\Delta\bar{g}_{Re}$  is the molar Gibbs free energy of the reaction, defined as the difference between the products energy and the reactants one. From the (2.11), it is possible to obtain the most general one:

$$Emf = E^0 + \frac{RT}{z_e F} \ln \frac{\prod^R (a_i)^{\nu_i}}{\prod^P (a_i)^{\nu_i}} \quad (2.12)$$

where  $E^0$  is the  $Emf$  at standard pressure and  $a_i$  is called activity, which corresponds to the ratio of pressure in case of ideal gases. Here all the passages are not described, but further information can be found in [15]. Considering the general equation (2.1), it is possible to derive the Nernst equation at the anode:

$$Emf = E^0 + \frac{RT}{z_e F} \ln \frac{(p_{H_2Oan})}{(p_{H_2an} \cdot p_{O_2cat}^{0.5})} \quad (2.13)$$

where the second term contains the partial pressure of steam and hydrogen at the anode and oxygen at the cathode. Once the circuit has been closed, the situation changes: there is the passage from the equilibrium domain to the transport phenomena, which can be distinguished in three main categories:

- charge transfer;
- charge migration;
- mass transport;

Those three phenomena are connected to effects of irreversibility, affecting the value of voltage, called over-potential.

**Activation over-potential** : The first one, activation over-voltage or over-potential,  $\eta_{ACT}$ , is linked to the activation energy ( $E_a$ ), which is needed to activate the charge transport and has to be taken from the OCV, as well explained in James et al. [15].

**Ohmic over-potential** : The second one, ohmic over-voltage or over-potential,  $\eta_{OHM}$ , related to the ions migration in conducting materials, which takes place mostly in the electrolyte layer and depends on the thickness of it.

**Diffusion over-potential** : Finally, the third one, called diffusion over-voltage or over-potential,  $\eta_{DIFF}$ , is present in the region of very high current, is related to the fact that molecules are not fast enough to continuously substitute the already reacted ones, so the concentration of the reactants decrease as well as the voltage, according to the Nernst equation 2.13.

Taking into account those losses, the voltage of the cell operating with current can be written as follow:

$$U_c = OCV - \eta_{ACT} - \eta_{OHM} - \eta_{DIFF} \quad (2.14)$$

The losses in voltage and the three regions of interest can be easily recognize just looking at the polarization curve (fig. 2.3).

That figure represents, in general, a polarization curve for a fuel cell device; talking about high temperature SOFC, the activation over-potential is playing a minor role, so the curve presents an almost linear behaviour.

Furthermore, diffusion over-potential is limited for high values of current. For that reason, the cell voltage calculation is done simply using the following equation:

$$U_c = OCV - ASR \cdot i \quad (2.15)$$

where ASR is the area of specific resistance in  $[\Omega \cdot cm^2]$  and  $i$  is the current density, in  $[A/cm^2]$ .

In addition, the last point on the right represents the maximum current density,  $i_{max}$ , which can be calculated using the Faraday's law:

$$\dot{n}_{gas} = \frac{I}{z_e \cdot F} = \frac{i \cdot A_{cell}}{z_e \cdot F} \quad (2.16)$$

Faraday's law is not only useful to evaluate the maximum current, but also to know the molar flow of every single gas inside the cell, playing with the number of electrons  $z_e$ . Equation 2.16 is considering a fuel utilization (FU) equal to 1, but that is an ideal condition. FU is a parameter which indicates the percentage of fuel effectively reacting in the cell. It is defined as the ratio of eq. 2.16 of the significant fuel entering the cell, methane for biogas application, and the real amount of fuel going into the cell, obtained considering the volumetric flow of the total biogas and the molar fraction of the interesting fuel. Owing to the fact that Faraday's law considers only molar flow, sometimes a conversion from volumetric to molar flow is needed, through the ideal gas law:

$$p\dot{V} = \dot{n}RT \quad (2.17)$$

Finally, the fuel utilization can be written as:

$$FU = \frac{\dot{n}_{CH_4Faraday}}{\dot{n}_{CH_4in}} \quad (2.18)$$

Increasing the value of FU means having a higher rate of reaction of the fuel, because of the molar flow increase and, therefore, the partial pressure, involved directly inside 2.19. As studied by Achenbach et al. [17] and also by Liso et al. [18] the reforming rate of methane has an exponential behaviour, which strictly depends on the partial pressure of the previously mentioned gas, at least talking about steam reforming. Going up with the concentration of the fuel means having also a rise in the partial pressure, due to the fact

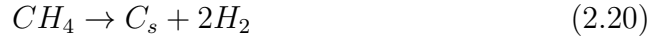
they are proportional (considering gases as ideal), as written in the fuel cell manual [13]. That rate is described by the following equation:

$$\dot{r}_{ref,i} = k_1 \cdot p_{CH_4,i} \cdot A_i \cdot e^{-\left(\frac{k_2}{RT}\right)} \quad (2.19)$$

where  $k_1$  and  $k_2$  are two constant, depending on activation energy, temperature and gas constant  $R$ ,  $A_i$  is the area of the cell and  $p_{CH_4}$  is the partial pressure of the methane.

### 2.1.2 Carbon deposition

The phenomenon of carbon deposition is caused by two reactions, the methane cracking (2.20) and the Boudouard reaction (2.21), forming carbon in a solid phase, called whiskers (tubes of 70-80 nm of diameter) which block the pores of the anode.



Since the pores are blocked, no more fuel is able to reach the TPB of the anode, but the ions of oxygen coming from the cathode side (due to the Faraday's law) are not influenced by this phenomena and so they continue to arrive at the anode: the result is a re-oxidation of the catalyst, passing from Ni to NiO. The problem is that size of NiO is larger than Ni, creating an increase of the anode size as well, which end up with stress in the material, especially in the layers near the electrolyte, leading to the fracture of the electrolyte layer: the cell is broken, since the reactants ( $H_2$  and  $O_2$ ) go in contact and burn. Assuming the second reaction, so the Boudouard one (2.21), as the most problematic one, it is possible to assess the carbon deposition value using the equilibrium constant of the previous mentioned reaction:

$$k_c = \frac{a_c \cdot p_{CO_2}}{p_{CO}^2} \quad (2.22)$$

where  $k_c$  is the equilibrium constant of the Boudouard reaction,  $p_{CO}$  and  $p_{CO_2}$  are the partial pressures respectively of  $CO$  and  $CO_2$  and  $a_c$  is the carbon activity.

The value of partial pressures of  $CO$  and  $CO_2$  can be calculated using Gibbs free energy minimization, taking advantage of the gases molar flow calculated:

$$\begin{cases} p_i = y_i \cdot p_0 \\ y_i = \frac{n_i}{n_{tot}} \end{cases} \quad (2.23)$$

This is exactly what has been done, using the same program written in Python as before, through a Python program, with a particular sub-function dedicated to the evaluation of  $a_c$  (for more details see H. Langnickel [10]). The value of  $a_c$  identifies a threshold value in 1, which separates the two zones:

- $a_c < 1 \rightarrow$  carbon deposition is not possible (thermodynamically not feasible);
- $a_c \geq 1 \rightarrow$  carbon deposition can occur;

In order to avoid this effect, an oxygen carrier (also called reforming agent) has to be added when dealing with hydrocarbon fuels. There are three possible reforming agent:  $H_2O$ ,  $CO_2$  and  $O_2$ ; the general evolution of carbon deposition with respect to the amount of C, H and O is reported in the next figure (2.4):

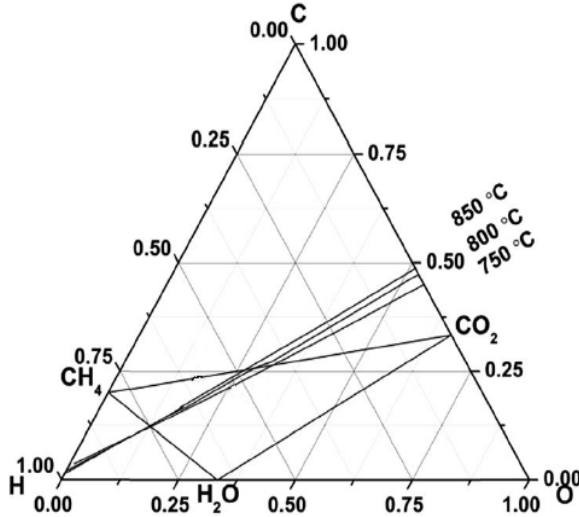


Figure 2.4: Carbon deposition boundaries (adapted from [19])

It is also clear from the previous figure 2.4 that carbon deposition depends on the cell temperature: the higher it is, the smaller is the problematic

area due to the fact that the equilibrium of the two reactions 2.20 and 2.21 is shifted towards the left at high temperature. In this work, the chosen temperature is  $750^\circ\text{C}$ . Another parameter which has a positive effect on carbon deposition is the amount of current delivered by the cell, as described more in detail in 3.1.1.

In normal conditions, so without recirculation, an extra amount of  $\text{CO}_2$  has to be added to the fuel mixture with the aim of avoiding that problem. Doing that, even at OCV, the value of  $a_c$  is really low.

### 2.1.3 Fuel recirculation: advantages and principal aim

Recirculation in a SOFC means re-utilize a part or the total amount of exhaust gases, exiting from the anode side in this case, which are still rich of fuel gases, such as  $\text{H}_2$ ,  $\text{CO}$  and  $\text{CH}_4$ , and reforming agent, so  $\text{CO}_2$  and  $\text{H}_2\text{O}$ , since oxygen is completely consumed inside the cell. The principal aim is to avoid carbon deposition ( $a_c$ ), which leads to the break down of the cell. The idea behind this thesis is to switch from extra  $\text{CO}_2$  to recirculation flow: in other words, in the first step a certain amount of extra  $\text{CO}_2$  is injected into the cell, but from the second step on that flow is substituted with the one coming from recirculation.

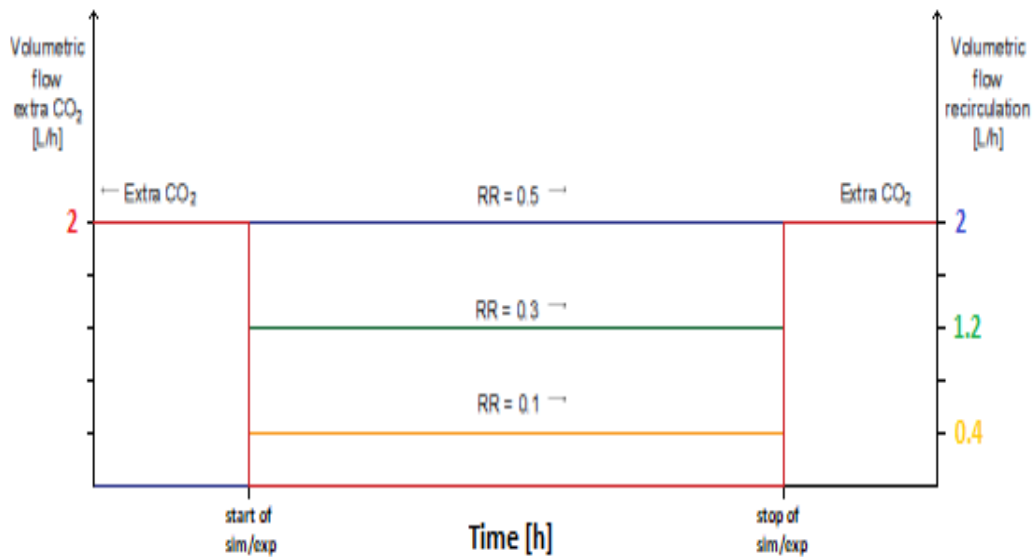
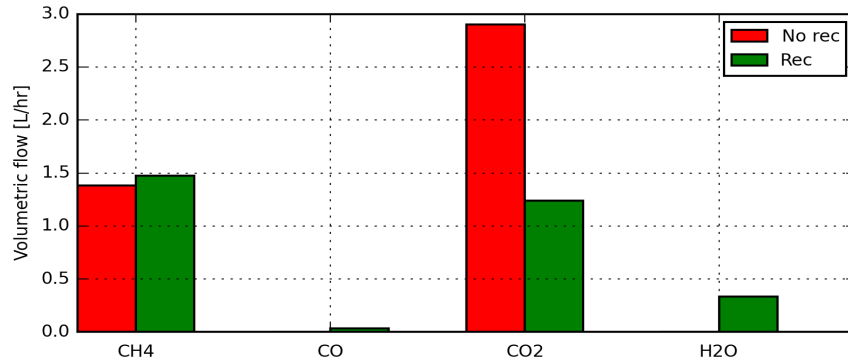


Figure 2.5: Scheme of the recirculation implementation

The composition of the recirculated flow is no more 100%  $\text{CO}_2$ , but it contains a mix of various gases, such as  $\text{H}_2$ ,  $\text{H}_2\text{O}$ ,  $\text{CO}$ , and  $\text{CH}_4$ , due to

the fact that the fuel utilization is not unitary, so a part of the methane is not reacting, while the amount of  $O_2$  is very low or null. Another advantage of using recirculation is the increase of the efficiency, as proved by Ralph-Uwe et al [8] and Dang et al [20]. This gain is mostly caused by the fact that some hydrogen exiting from the anode is partially recirculated and can be re-used, increasing the fuel utilization. On the other hand, there are a few disadvantages, because some  $CH_4$  and  $CO$  are recirculated, increasing the problem of carbon deposition, which now not only depends on methane (2.20), but also on carbon monoxide, because of Bouduard reaction (2.21). This effect is attenuated by the fact that also a certain amount of  $CO_2$  and  $H_2O$  are present in the exhaust gases (with a percentage that varies according to the RR) and so recirculated (fig. 2.6), but the value of  $a_c$  is higher than the initial one (in which extra  $CO_2$  is used).



**Figure 2.6: Volumetric flows with and without recirculation**

To be more precise, the carbon activity strongly depends also on the composition of the biogas, and especially on the quantity of methane and carbon dioxide, and on the FU of the cell, which indicates the percentage of methane reacting. A low value of recirculation rate could be used in the case of low methane content biogas, where recirculation is almost not needed, but it should be done in order to homogenize the carbon activity along the cell, avoid having a strong peak in the first sub-cell (sub-cells), which can affect negatively the performance of the cell, leading also to a failure. From the opposite point of view, a high value of RR means having a very low  $a_c$ , comparable to the one obtained using the extra amount of  $CO_2$ , but it carries some problems related to faster degradation of the cell and lower fuel

utilization, which affect the efficiency of the system (as studied by Dang et al [20]). The degradation of the cell is something which has to be taken into account, caused by the gas itself and enhanced by the presence of water: steam, in fact, is a good reforming agent and temperature regulator (due to the fact that 2.4 is endothermic, so it adsorbs heat), but it also increases the damages to the cell.

### 2.1.4 Power and efficiency of a fuel cell

In order to evaluate the performance of a fuel cell, the efficiency and the power must be calculated: as regards the first one, it is defined as the ratio of power produced by the cell and power of the fuel (eq. 2.24).

$$\eta_{el} = \frac{P_{cell}}{P_{fuel}} \quad (2.24)$$

The power delivered by a fuel cell is the product of current density, area of the cell and voltage if a single cell is considered.

$$P_{cell} = I \cdot U_c = iA_{cell} \cdot U_c \quad (2.25)$$

measured in Watt [W]. It is clear that the power depends on the dimension of the cell and also on the fuel utilization, which is linked to the current density as shown in eq. 2.18. The power of the cell has then to be compared with the theoretical one that can be obtained from the fuel molar flow entering at the anode, defined as the product of molar flow and Low Heating Value (LHV), in [J/mol], of the used fuel:

$$P_{th} = \dot{n}_{fuel} \cdot L\bar{H}V_{fuel} \quad (2.26)$$

Substituting eq. 2.25 and 2.26 in the efficiency one (2.24):

$$\eta_{el} = \frac{iA_{cell} \cdot U_c}{\dot{n}_{fuel} \cdot L\bar{H}V_{fuel}} \quad (2.27)$$

## 2.2 Biogas

Biogas is a type of gas recovered from organic matter, making use of biochemical processes, involving bacteria or enzymes (operating at about  $T_{amb}$ ). In general, it consists of a mixture of  $CH_4$  (50 – 80%) and  $CO_2$  (30 – 50%), with more than 500 contaminants, including sulfur ( $H_2S$ ), siloxanes ( $SiO_2$ ) and halogenous, which are also called bad contaminants, and  $H_2O$ ,  $N_2$ ,  $O_2$ , that are not problematic for the cell. The composition of the biogas depends on the initial matter from which it comes from, typically waste water, animal waste, agriculture waste or landfill. The recovery of biogas is a good practice not only from the energy point of view, due to the fact that it contains quite a lot of methane, but also from an environmental point of view, since it is a greenhouse gas and its release into the atmosphere has to be avoided. A typical gas composition of the various type of biogas is reported in table 2.7, with a comparison to Natural Gas (NG) composition.

Composition	Natural gas	Biogas			
		Waste water	Food waste	Animal waste	Landfill
Methane [% vol.]	80 – 100	50 – 60	50 – 70	45 – 60	40 – 55
Carbon dioxide [% vol.]	< 3	30 – 40	25 – 45	35 – 50	35 – 50
Nitrogen [% vol.]	< 3	< 4	< 4	< 4	< 20
Oxygen [% vol.]	< 0.2	< 1	< 1	< 1	< 2
$H_2S$ [ppm]	< 0.1	< 400	< 10'000	< 300	< 200
Non $H_2S$ sulfur [ppm]	< 10	< 1	< 1'000	< 30	< 30
Halogens [ppm]	< 0.1	< 0.2	< 0.2	< 0.2	< 100
Moisture [%]	< 0.02	~ 3	~ 3	~ 3	~ 3

Figure 2.7: Different biogas composition with respect to NG

### 2.2.1 Contaminants

Dealing with real biogas, the problem of contaminants has to be taken into consideration, due to the damaging they can cause, and it has been studied quite a lot in the literature ([21], [22]). In particular, landfill biogas is rich in sulfur (due to  $H_2S$ ), which not only poisons the reforming activity inside the cell, but also the electrochemical reaction (as studied by Hagen et al.

[4]), leading to a rapid drop of the cell voltage and increment of resistances, especially polarization one ( $R_p$ ). In order to avoid the contamination of the cell from  $H_2S$  or other contaminants, an activated carbon filter should be used in order to clean the biogas before entering the cell: unfortunately, the efficiency of that filter is not unitary, so a small quantity of undesired compounds can reach the cell, leading to faster degradation. Moreover, even if nitrogen is not considered as a dangerous contaminant for the cell since it does not lead to any damage, it dilutes the fuel, which means lower partial pressure and, therefore, a lower voltage (according to 2.13) and power output. Landfill biogas contains a very high amount of  $N_2$ , so this parameter has to be evaluated carefully.

### 2.2.2 Type of biogas analyzed

In this work, three types of biogas have been studied with the composition of landfill, waste water and animal waste biogas. Firstly, pre-mixed biogas has been considered, created just mixing  $CH_4$ ,  $CO_2$  and  $N_2$  (via mass flow controller in the laboratory), in which impurities, such as sulfur, are not present, so a filter is not needed. The last test, though, is carried out with real biogas, coming from Odense Renovation, and this time the flow needed to be filtered through an activated carbon filter, to take out sulphur especially. The composition of the three biogas is reported in table 2.1.

Composition	Type of Biogas		
	Landfill	Animal Waste	Waste Water
$y_{CH_4}$	0.345	0.48	0.641
$y_{CO_2}$	0.225	0.48	0.315
$y_{N_2}$	0.43	0.04	0.044

Table 2.1: Composition of the three biogas (from [23] and [7])

Regarding the real biogas, the composition should be the same of the pre-mixed one, but due to the fact that anaerobic digestion presents some fluctuations, the amount of methane can be higher or lower than expected.



# Chapter 3

## Theoretical study

The following chapter is dedicated to the description of the simulation part of this thesis, in which the so called pre-mixed biogas is used: the gas is created just adding the desired amount of  $CH_4$ ,  $CO_2$  and  $N_2$  and it is easier to manage due to the fact that impurities, such as the previously described in 2.2.1, are not present. Pre-mixed biogas will be used both for landfill and waste water biogas.

### 3.1 Simulation set up

#### 3.1.1 Simulation description

In this thesis the first aim is not to have carbon deposition at the anode side of the cell, so the thermodynamic chemical equilibrium is evaluated, taking into account only the gas phase of the various species, assuming the solid one as null. Dealing with a system in which more than a single reaction is taking place, a minimization of the Gibbs free energy is needed in order to find out the equilibrium composition, as has been studied from Jooh-Ho et al [9] and da Silva et al [11]. The minimization has to be done with respect to  $j$  species ( $n_j$ ), at a constant temperature and pressure. Working with biogas, the expected species inside the cell are assumed to be the six, reported in tab. 3.1.

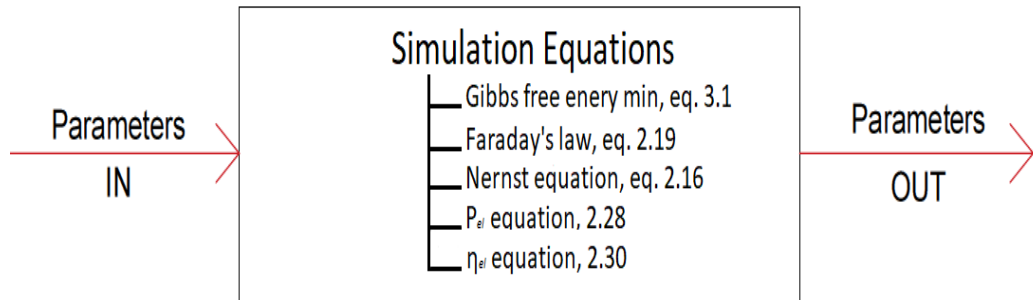
Owing to that number of species, for the theoretical simulation of recirculation a program written in Python 2.7 has been used, with an in-house design function developed by Langnickel ([10]) for the evaluation of the composition through the Gibbs minimization, deriving the formula 3.1 with respect to  $n_j$ :

$$\min(dG_{system}(dn_j))_{T,p} = 0 \quad (3.1)$$

Species	Description
$CO_2$	Carbon dioxide
$CO$	Carbon monoxide
$CH_4$	Methane
$N_2$	Nitrogen
$O_2$	Oxygen
$H_2$	Hydrogen
$H_2O$	Water (Steam)

Table 3.1: Table of species

As regards the way in which the simulations are performed, a scheme has been reported in fig. 3.1.

**Figure 3.1: Scheme of simulation**

Changing the parameters in input, the internal simulation varies and, therefore, the output parameters. The code has been written in order to have a lot of possibilities in terms of analysis, just modifying some input parameters. A resume has been reported in tab. 3.2

<b>Parameters IN</b>	<b>Parameters OUT</b>
Biogas composition	Carbon activity
Nr of sub-cells	Efficiency
Fuel utilization	Voltage
Recirculation Rate	Power
ASR	Gas composition
Extra $CO_2$	Molar fractions
Cell temperature	
Cell pressure	

Table 3.2: Simulation parameters

Cell temperature and pressure have been kept constant for every simulation run, as well as the extra amount of  $CO_2$  initially used. Moreover, the area of specific resistance has been taken as an average of the previous experiments done in the rig (for landfill and waste water). In tab. 3.3 all the values used are reported.

<b>Parameter</b>	<b>Value</b>
Biogas composition	Landfill-Waste water
Nr of sub-cells	10
Fuel utilization	0.6-0.8
Recirculation Rate	0-0.5
ASR	0.39-0.435 [ $\Omega \cdot cm^2$ ]
Extra $CO_2$	2 [L/h]
Cell temperature	750 [ $^{\circ}C$ ]
Cell pressure	101325 [Pa]

Table 3.3: Input parameters value

The software simulate a real SOFC, with three entrances, one for biogas, one for the initial extra  $CO_2$ /recirculated flow and the last one for the  $O_2$ , since the oxygen coming from the cathode side is considered as an external flow entering the cell, and an exit, for the exhausts. A scheme of the cell is shown in figure 3.2:

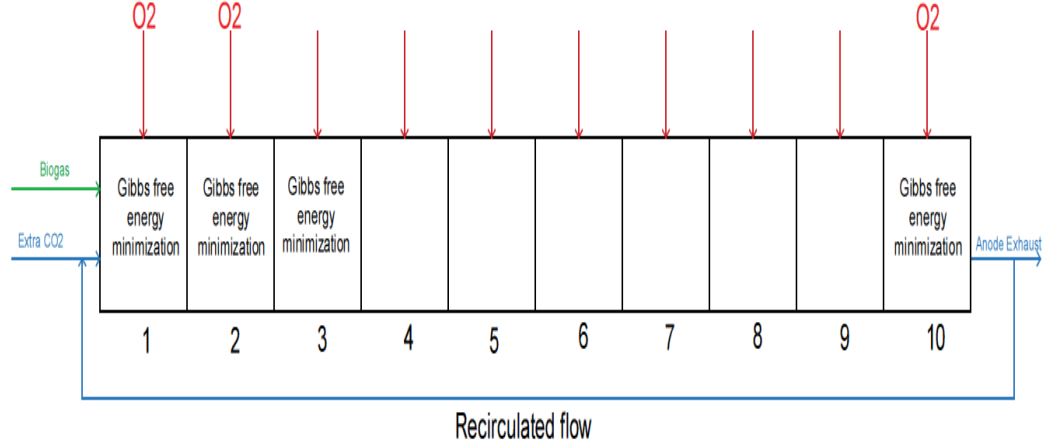


**Figure 3.2: Scheme of the virtual SOFC**

In the present study the cell has been divided in ten sub-cells, in order to understand the problem with a semi-1D model (similar to what has been done by Liso et al [18]), considering only thermodynamics and no kinetics. In each sub-cell a certain amount of oxygen (coming from the cathode side) is injected, following the equation:

$$n_{O2(sub-cell)} = \frac{1}{n_{cells}} \cdot n_{O2(total)} \quad (3.2)$$

where  $n_{cells}$  is the number of sub-cells, equal to 10 in this case, and  $n_{O2(total)}$  is the oxygen quantity deriving from Faraday's law (2.16). After that, the Gibbs free energy minimization is applied to every cell. The Python program has been modeled to permit a change in the number of sub-cells: although the result is more precise using a higher value of sub-cells, the computational time increases. Ten is the right compromise between an accurate simulation and an acceptable computational time. Furthermore, the simulation takes into account different number of steps, starting from the first one in which biogas (4 L/h) and extra  $CO_2$  (2 L/h) are injected, and going on, substituting the extra  $CO_2$  flow with the recirculation one (2.5), until when the flow is stable. Simulation is then stopped making use of a while loop, a tolerance and an error, the last one calculated as:

$$Err_{rel} = \frac{|a_{c_{max}}[i] - a_{c_{max}}[i-1]|}{|a_{c_{max}}[i]|} \quad (3.3)$$

where  $i$  stands for the number of steps computed. Tolerance and error are applied to the carbon activity (calculated through 2.22) of the first sub-cell,

which is the most problematic one since the  $a_c$  is higher there due to the fact that the amount of methane is high, while the quantity of reforming agents and  $O_2$  are not. The while loop stop when the carbon activity is stable.

The way to proceed in this section has been divided into two parts: the first one is dedicated to more general simulations, in order to understand:

- the impact of variation of fuel utilization and, as a consequence, of the current density (2.16 and 3.4);
- the impact of variation of the biogas composition;

the second part is an analysis in depth of the most interesting conditions, paying particular attention to:

- carbon activity along the cell;
- voltage, electric power and efficiency output;

As mentioned in previous paragraphs, the amount of current influences the carbon deposition and obviously also the electrical power output of the cell, directly connected with the efficiency. The quantity of oxygen coming from the cathode side is easy to find out using the Faraday's law (2.16), in which the number of electrons,  $n_e$ , is equal to 4. In this work different simulations has been carried out in a range of current between 8 A and 14.72 A (0.5-0.92 A/cm<sup>2</sup>), according to what has been examined in literature in terms of fuel utilization, observing a very high influence of I. As already studied by Jooh-Ho et al [9], working with a certain amount of current help to reduce consistently, or not have, carbon deposition, since not only the oxygen will form  $CO_2$ , but also it reacts with hydrogen forming another reforming agent: steam (see 2.4). On the other hand, this is not sufficient to guarantee the safety of the cell in its entire length, due to the fact that the composition of the gases change along it. Again, the most problematic part is the first sub-cell (or better the first two-three sub-cells) where the amount of oxygen is not so high and the quantity of  $CH_4$  is the maximum one. For those reasons, the first sub-cell has been taken as the reference to show the variation of the carbon activity with i (fig. 3.3).

Regarding the variation of recirculation rate, it has been considered referring to the volumetric flow of biogas, which has been kept constant (4 L/h), as well as the extra  $CO_2$  amount. Owing to the fact that 2 L/h of extra  $CO_2$  represents the 50% of the biogas flow, at the beginning there is a variation of the total flow, which can increase if the recirculation ratio is higher than 50%, decrease if it is lower or remains constant if exactly 50% of recirculation

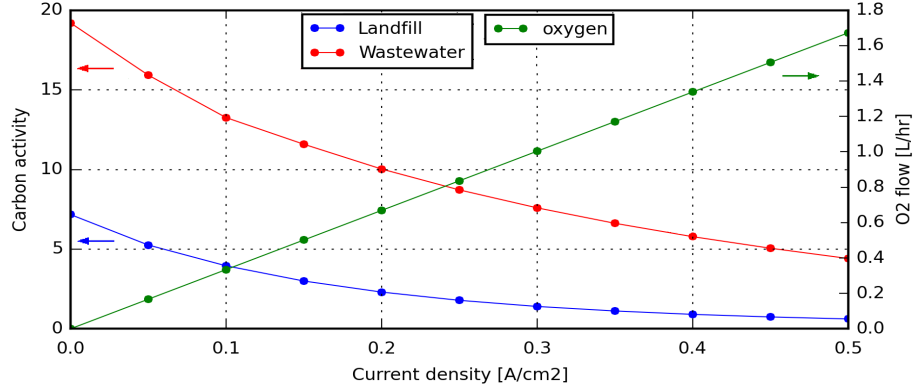


**Figure 3.3: Carbon activity behavior with current and 50% of recirculation**

is applied. In any case, after one step the total flow becomes constant again, no matter which RR has been used. The amount of oxygen flow is constant and depends only on the current used, so on the FU (eq. 2.18) as shown in fig. 3.3. For the calculation of the volumetric flow, the ideal gas law has been considered (eq. 2.17).

Another parameter which influences the carbon activity is the composition of the biogas injected into the cell. Using, for example, different types of biogas (landfill, waste water), the amount of  $CH_4$ ,  $CO_2$  and also  $N_2$  changes, heading to different results. In the simulation part, three different biogas have been analyzed, with the composition already cited in chapter 2. In particular, more attention has been paid at the first two type of biogas, since the landfill one has a low content of methane and high content of nitrogen, while the waste water one presents the opposite characteristics. The amount of  $CO_2$  is a little bit higher in the waste water and the extra  $CO_2$  is kept constant for both at the first step for two main reasons: it has been proved through simulations that are sufficient to avoid problems of carbon deposition, and secondly, the idea was to maintain the same initial conditions for each type of biogas, to have a more accurate analysis. It is expected that the average carbon activity in the second case results to be higher since the  $CH_4$  is almost the double. This is actually not always true, due to the fact that, depending on the current used, some methane could not react and simply pass through the cell. The parameter that influences the amount of methane

reacting in the cell is the previously described fuel utilization. For  $CH_4$ , the Faraday's equation is the 2.16, with a number of electrons involved,  $n_e$ , equal to 8 for this hydrocarbon. In order to better understand the trend of carbon activity changing the recirculation rate, in the simulations the value of fuel utilization has been fixed, according to what is done in the literature (Engelbracht et al. [24]), varying then the amount of current. Each simulation FU parameter and the corresponding current density has been summarized in table 3.4.

	Landfill		Animal Waste		Waste Water	
FU	0.6	0.8	0.6	0.8	0.6	0.8
$i [A/cm^2]$	0.495	0.66	0.689	0.918	0.92	1.226

Table 3.4: FU-current density

The two values of the fuel utilization have been chosen since they are significant in terms of literature. Passing from the landfill composition to the waste water one, the current density is more than doubled, due to the fact that a high current is needed to take advantage of the high methane content biogas. The carbon activity has been evaluated considering the first sub-cell, due to the reasons already explained in previous paragraphs. In the following graphs, the  $a_c$  dependence on RR and FU is illustrated for every pre-mixed composition.

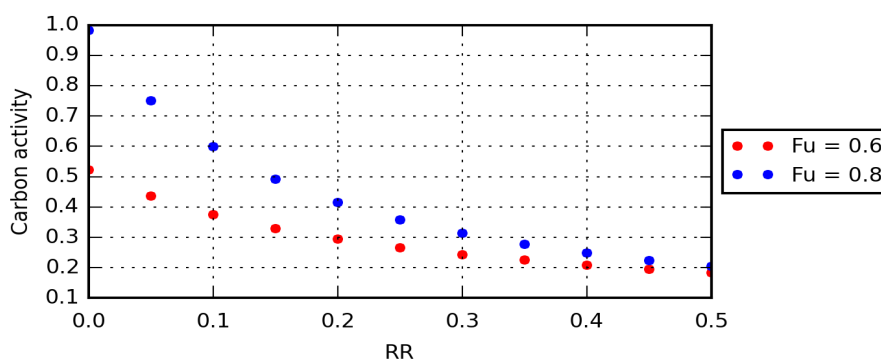


**Figure 3.4: Landfill: carbon activity behaviour depending on RR with different FU**

It is interesting to note that for the landfill biogas (fig. 3.4) using a FU

equal to 60% recirculation is not needed, since the oxygen generated due to the current and the amount of  $CO_2$  already contained in the biogas are sufficient to avoid high carbon activity which should intact the cell. A different situation appears if the FU is increased up to 80%: in this case, without applying recirculation, the value of  $a_c$  is almost 1, so just a small fluctuation on the gas composition can lead to the formation of carbon particles on the cell anode. Due to that, it is highly recommended to recirculate at least 10% of the flow and, to be sure, is even better going up to 20%. In addition, even if it is not necessary to recirculate in the case of low fuel utilization, it should be done if possible, in order to homogenize the gas composition along the cell.

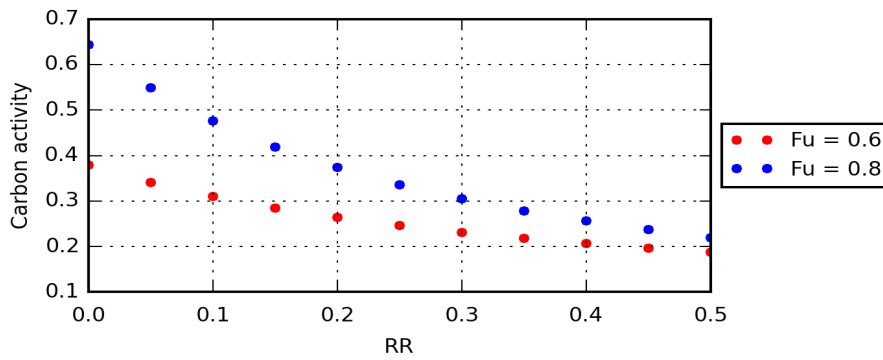


**Figure 3.5: Animal Waste: carbon activity behaviour depending on RR with different FU**

Animal waste biogas (fig. 3.5) results to be the less appealing in terms of fuel recycling, due to its composition, reach in  $CO_2$ , which is enough to avoid carbon particles. For low FU, recirculation is definitely not needed, while it is suggested for values above 80%, just to be sure in case of fluctuations. Since from this preliminary analysis it looks the less interesting one, it has been not examined in depth.

Finally, waste water biogas (fig. 3.6) results to be the most intriguing of the three: with no recirculation, no matter which fuel utilization, the carbon activity overcomes the limit, as illustrated in fig. 3.6. In addition, using a low recirculation rate, the problem is not solved and there is the need to use at least a RR of 30%. For high fuel utilization is even better to reach a percentage of 40% to assure the safety of the system.

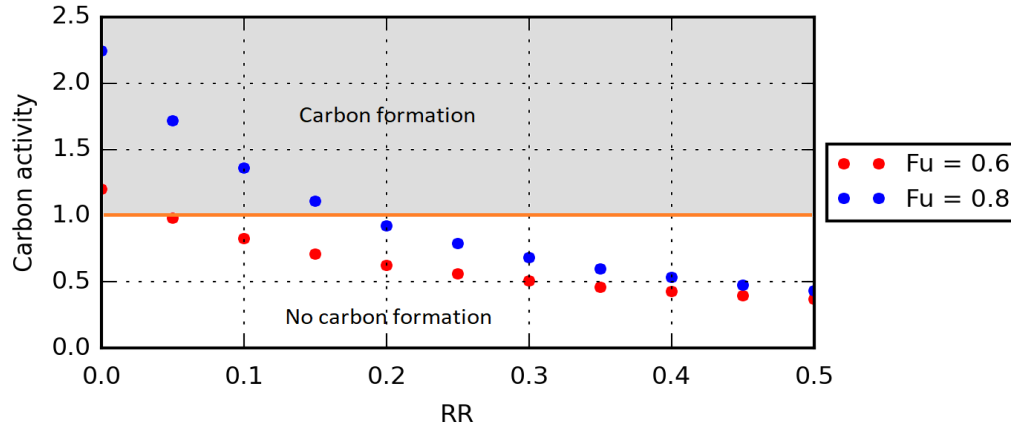


**Figure 3.6: Waste Water: carbon activity behaviour depending on RR with different FU**

### 3.1.2 Biogas anode fuel recycling study: simulation

According to table tab. 3.3, some experiments have been deeply analyzed. A brief overview of each simulation is reported in table 3.5.

Simulation nr.	Biogas	RR	$FU_{low}$	$FU_{high}$
1	Landfill	50	0.6	0.8
2	Landfill	30	0.6	0.8
3	Landfill	10	0.6	0.8
4	Waste water	50	0.6	0.8
5	Waste water	30	0.6	0.8
6	Waste water	10	0.6	0.8

Table 3.5: Pre-mixed biogas simulations overview

## 3.2 Results of simulations study

Each simulation has been carried out with the so called pre-mixed biogas, which has the same composition of the landfill or waste water biogas, but the advantage that it does not contain any impurities. The principal aim was to study the behaviour of the cell applying recirculation and, as a consequence, avoiding the use of extra  $CO_2$  during operation (fig. 2.5), limiting its adoption only for the start up and shut down of the experiment, since there are no possibilities to completely avoid it. The extra  $CO_2$  has the function of increasing the reforming agent, in order not to have carbon deposition, so the attention was on the value of  $a_c$  at first. The study has been conducted using values of current which assure a fuel utilization of 60% and 80%, in order to have a comparison with some articles in the literature. The first three simulations are done considering the landfill composition, while the last three considering the waste water biogas one. Other two tests, called test 0, have been done considering extra  $CO_2$ , in order to have a comparison. Everything is resumed in table 3.6, where voltage and electrical efficiency are reported as well, both for FU equal to 60% and 80%.

### 3.2.1 Landfill: pre-mixed biogas

test nr.	RR [%]	<i>FU</i> 0.6		<i>FU</i> 0.8		extra $CO_2$
		Voltage [V]	$\eta_{el}$	Voltage [V]	$\eta_{el}$	
0	0	0.759	0.439	0.702	0.542	yes
1	50	0.791	0.458	0.721	0.557	no
2	30	0.801	0.464	0.736	0.568	no
3	10	0.817	0.473	0.761	0.588	no

Table 3.6: Pre-mixed landfill simulations results in terms of voltage and efficiency, different FU

**Simulation 1** : The first case that has been examined was the one with a RR equal to 50%, the simplest one since the total flow does not change, due to the fact that 2 L/h were recirculated, and the same quantity of extra  $CO_2$  was taken out. The analysis of the carbon activity along the cell (fig. 3.8, blue line) shows a value which is very low: that line represents the  $a_c$  calculated in the last step, so the one in which stability has been reached.

The step denominated line "extra  $CO_2$ " (red line) is referred to the start up of recirculation, in which the extra carbon dioxide is added to avoid problems since it is not possible to recirculate from the beginning due to a lack of gases at the outlet of the cell. As expected, it presents the lower value of  $a_c$ , while stopping this extra  $CO_2$  and starting the test results in an increase of carbon activity of almost the double, but still far from the threshold value of one. Using a higher fuel utilization, FU equal to 80% (fig. 3.9), means going up a little bit with the carbon activity in the first part of the cell (+11%), but the most interesting observation is that the  $a_c$  of the red line (extra  $CO_2$ ) has almost the same value of the blue line, where recirculation is done and stable. This is important since it demonstrates recirculation has a better impact in case of high FU. The highest value of  $a_c$  is in proximity to the entrance of the cell, as expected, and it decreases almost to zero by the end of it. It is interesting to observe the trend of the various molar flow of the gases involved, here reported for the final step:

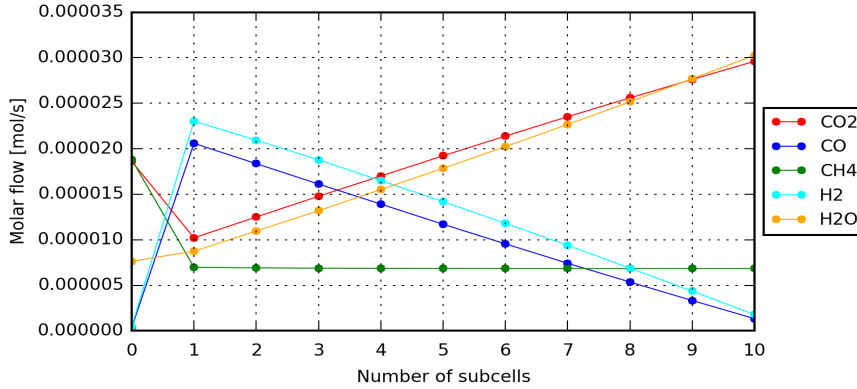


**Figure 3.7: Landfill: molar flows along the cell, final step  
FU = 60%**

An analysis of the methane behaviour inside the cell should be done: it follows an exponential law which is quite consistent with what Achenbach et al. [17] claim, even if the previously mentioned study has been developed for steam reforming, which is only partially present in this work. This trend seems not exponential, due to a high utilization of  $CH_4$  in the first sub-cell, that leads to something similar to a linear tendency. The difference could be caused by the fact that Achelbach et al. are only considering SR (eq. 2.4) and WGS reaction (eq. 2.7), while in the previous simulation, the big role

is played by the DR (eq. 2.5), due to the huge amount of carbon dioxide naturally present inside biogas. Regarding the other gases,  $H_2$  and  $CO$  are increasing in the first sub-cell, due to all the three previously mentioned reactions, while, once oxygen reaches the anode side, they decreasing forming steam and carbon dioxide. The quantity of hydrogen and carbon monoxide in the last sub-cell is very low since the amount of oxygen is almost sufficient to consume both of them. As regards the simulation with a  $FU = 80\%$ , the curves are similar, but shifted towards the upper part, except the methane one, which decreases, since more moles are reacting. For this reason, the amount of hydrogen and carbon monoxide go up at the beginning, being then converted in  $H_2O$  and  $CO_2$ . The total quantity of these last two gases is also higher due to the fact that working with a bigger  $FU$  results in having a higher current density (tab. 3.4) and so more oxygen available inside the cell. That is also the reason why the carbon activity is slightly higher (11%) in this second case only in the first sub-cell and not in the totality of the ten: reacted methane is higher, but steam and  $CO_2$  are increased as well.

Finally, the performance of the cell has been analyzed, paying attention especially to the voltage and the efficiency, compared to the extra  $CO_2$  case (tab. 3.6). According to Dietrich et al. [8] and Saebea et al. [20], the voltage and, as a consequence, the efficiency should increase, due to the fact that some methane and hydrogen are recirculated. The voltage has been calculated according to equation (2.15) and considering an  $ASR$  equal to 0.435, which is aligned with experimental data analyzed from Hagen et al. [5]. There are two columns, dedicated to the study of the lower fuel utilization, so 60%, and to the analysis of the higher one, 80%.

In both cases, there is an increase of the voltage, which results in a growth of efficiency of 4% considering the lower  $FU$  and 3% for the higher one. The last case has a smaller efficiency, since the gain in voltage is not so high (20 mV, with respect to the 32 mV of the other one) and the current density plays a fundamental role regarding the losses, due to 2.15, decreasing the power. So in this simulation, the current has the key role, which leads to a better performance.

**Simulation 2** : Considering the result of simulation 1, reducing the  $RR$  to 30% is possible, as shown in figure 3.8, green line. On one hand, reduction of  $RR$  means going down with the steam flow, leading to a lower degradation rate, but on the other hand, the amount of  $H_2$  recirculated is lower, expecting a decrease of the voltage, in theory. The  $a_c$  is again reported in fig. 3.8. According to the expectations, the growth of carbon activity is higher than before, passing from 0.1 to almost 0.25, so increased of 250%.

Despite everything, the situation is not problematic and the cell can run in a safe environment. For the 80% FU case,  $a_c$  results to be higher (approximately the double), but with a lower difference with respect to the case "0", confirming that recirculation has a better impact in high FU experiments as previously mentioned. Here the molar flows along the cell have not been reported, because they are quite similar to the previous ones. Obviously, the quantity of  $H_2$  and  $CO$  is reduced, due to the fact that less biogas is recirculated, and, as well, the amount of  $H_2$  and  $CO_2$  produced. Regarding the voltage, it surprisingly results to be higher than the previous case as well as the efficiency. This is caused by the fact that the total amount of flow is lower applying the recirculation (5.2 L/h) than the initial one with extra  $CO_2$  (6 L/h), so the fuel is less diluted and the voltage increase. According to the Nernst equation (2.13), having a less diluted mixture entering the cell means the partial pressure is higher, resulting in a bigger voltage since the two are proportional. The value of voltage and efficiency are reported in table 3.6. For both values of FU, the increase in efficiency is around 5%, so higher than the previous one (RR = 50%).

**Simulation 3** : Reducing the RR even to 10%, as illustrated in figure 3.8, yellow line, is also possible. It is clear that now the difference between the extra  $CO_2$  case and recirculation one is really huge, with an increment of carbon activity of more than 3.5 times, but the cell can still work in safe conditions. Different is the case of 80% of fuel utilization, where the  $a_c$  is practically 0.6, so a fluctuation of the gases feeding the cell can cause damage to it, especially due to the fact that the slope of the curve representing the carbon activity is quite pronounced, so a small variation of the recirculation rate can create a big deviation of  $a_c$ . As already explained in the previous section, a recirculation of 10% is the minimum required to be sure not to have problems in case of high FU. Voltage and efficiency present a quite consistent rise, as can be seen in table 3.6. The gain in efficiency is 7% for FU of 60% and 8% for the other case, making this case the most interesting one from the efficiency point of view, so close to 60%.

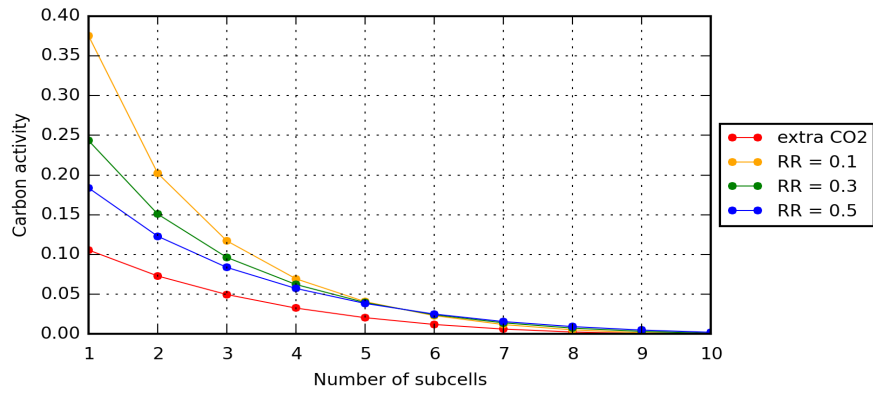


Figure 3.8: Landfill: carbon activity with respect to RR,  
FU = 60%

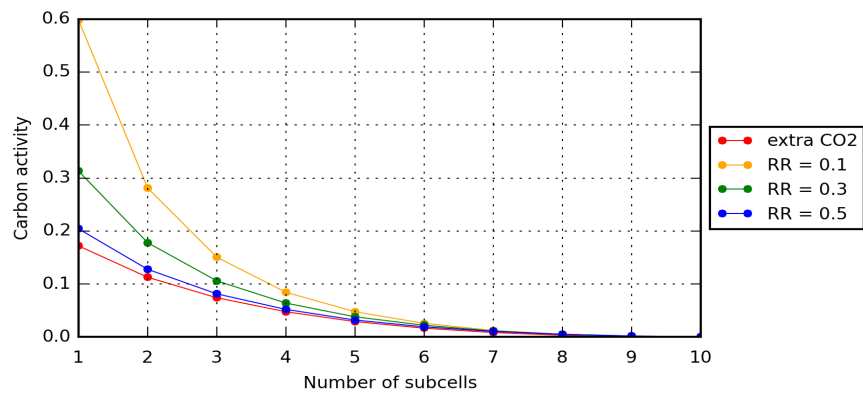


Figure 3.9: Landfill: carbon activity with respect to RR,  
FU = 80%

### 3.2.2 Waste water: pre-mixed biogas

The second part of the simulation is dedicated to the other pre-mixed biogas, the one with the same composition of waste water biogas, reported in tab 2.1. The amount of methane is almost the double, so the carbon activity is expected to be higher, even if it contains a higher quantity of  $CO_2$ .

test nr.	RR [%]	<i>FU</i> 0.6		<i>FU</i> 0.8		extra $CO_2$
		Voltage [V]	$\eta_{el}$	Voltage [V]	$\eta_{el}$	
0	0	0.601	0.348	0.485	0.375	yes
4	50	0.622	0.360	0.493	0.381	no
5	30	0.634	0.367	0.511	0.394	no
6	10	0.653	0.378	0.538	0.415	no

Table 3.7: Pre-mixed wastewater simulations results in terms of voltage and efficiency, different FU

**Simulation 4** : In order to follow the same procedure of the landfill case, a recirculation ratio of 50% has been used in the first simulation. As expected also the  $a_c$  considering the extra  $CO_2$  is more than the double with this type of biogas and the same happens if the recirculation is considered with a FU of 60% (fig. 3.11), but there is no risk for the cell, since the threshold limit is quite far. The interesting thing can be seen in the high FU graph (fig. 3.12), where there are no differences in  $a_c$  applying the 2 L/h of extra  $CO_2$  or recirculation since the blue curve is overlapping the red one. Being more precise, the carbon activity is even lower in the second case. This can be explained just paying attention to the molar flow of steam (fig. 3.10), which is extremely high, avoiding any possibilities of carbon deposition at the anode due to steam reforming.

The amount of methane is higher due to the recirculation, but the quantity of  $CO_2$  has increased as well and, in addition, there is a consistent flow of steam, which has a stronger impact on carbon activity reduction. Similarly to the landfill pre-mixed case, the flows of hydrogen and carbon monoxide react almost totally by the end of the cell, leading to a null value of  $a_c$ . The OCV is bigger than before, but it does not result in a higher cell voltage since the value of current used, to have a fuel utilization of 0.8 (tab 3.4), enhances the second member of equation 2.15, so ohmic losses. There is a rise of voltage and efficiency, but, as well as in the landfill case, not so consistent,

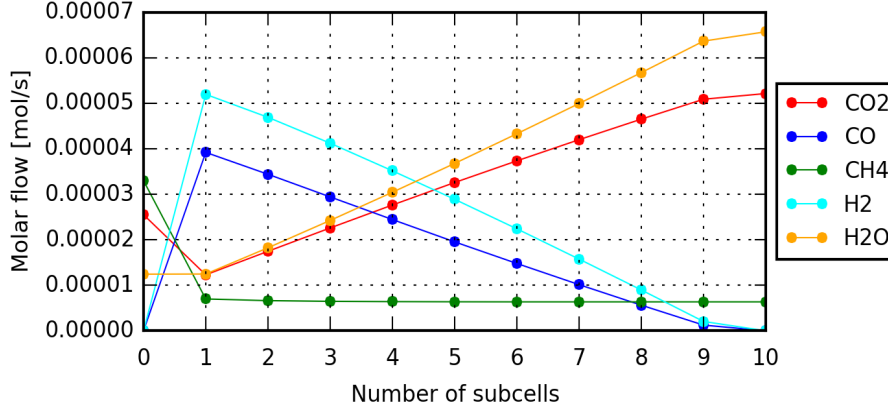


**Figure 3.10: Waste Water: molar flows along the cell, final step FU = 80%**

resumed in tab. 3.7. The gain in efficiency is 3% in the low FU case and only 2% in the other one.

**Simulation 5** : Carbon activity using waste water composition have been demonstrated to be considerable in the last simulation, close to the threshold. So, according to the previous simulation, the recirculation rate has been reduced to 30% and the results are illustrated in figure 3.11, green line. This graph is more similar to the Landfill ones, since the recirculation has a higher value of carbon activity with respect to the initial step, with a growth of almost 50%. The threshold level is not overcome yet, but the first sub-cell is not so far from the risky operation condition. This means that in case of problems related to the fuel entering in the cell or to the recirculation branch, there could be carbon deposition. Regarding voltage and efficiency, everything is reported in table 3.7. Even in this case the voltage results to be higher than the previous simulation, due to the less diluted fuel. Efficiency gain is comparable to the landfill one. There is an increase of 5% considering both FU. The value of efficiency stays between 0.3 and 0.4, so not surprisingly high, but this is caused by the fact that the current is high and therefore also the ohmic losses. Increasing the fuel utilization over the studied ones helps efficiency growth, but at the same time recirculation becomes not sufficient to avoid high  $a_c$ . Therefore, recirculation with RR of 30% is applicable only for small value of fuel utilization.

**Simulation 6** : Finally, just to complete the general view, also a simulation with only 10% of RR has been run, expecting to overcome the carbon activity limit. Again, results are illustrated in figure 3.11 and 3.12, yellow line, for both the FU considered. Looking at the first sub-cell for the high fuel utilization case, the value of carbon activity is abundantly above the threshold limit, therefore it is not possible to apply a so low recirculation ratio, or at least some reforming agent has to be added again, but in contrast with one of the aim of this thesis (which is eliminate injection of no combustible external sources). The situation is not getting better with a lower FU, as the value of  $a_s$  is, of course, lower than 1, but it stays between 0.8 and 0.9: working in this conditions is not recommended. For good knowing, voltage and efficiency have been reported in tab. 3.7. The outcome is really interesting, with a growth of the efficiency of 10% if 0.8 is considered as fuel utilization, but this is not feasible due to carbon formation.

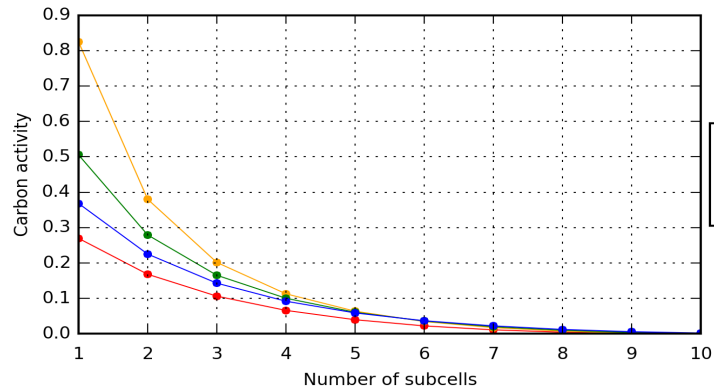


Figure 3.11: Waste water: carbon activity with respect to RR,  $FU = 60\%$

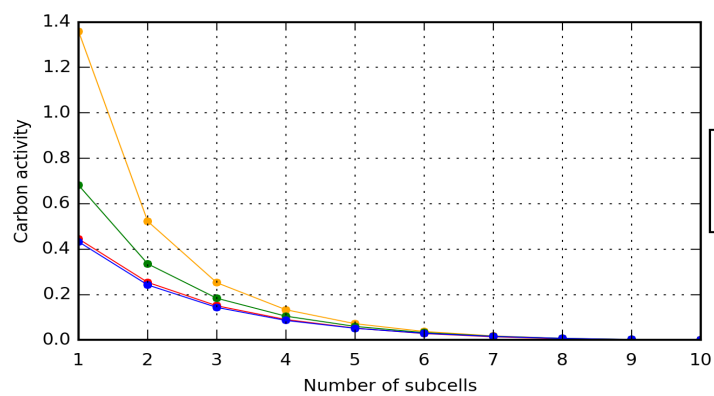


Figure 3.12: Waste water: carbon activity with respect to RR,  $FU = 80\%$

# Chapter 4

## Experimental study

### 4.1 Experimental set up

In order to better understand the behaviour of recirculation in a real fuel cell and also to prove the validity of the simulations, some laboratory tests on cell level have been carried out. The first part, called "pre-mixed" recirculation, consists in simply adding the amount of gases coming from simulations to the anode of the cell via mass flow controllers (MFC), in order to simulate the recirculation. Then, the four last experiments have been carried out using a pump to recirculate directly the gases, according to the scheme reported below (fig. 4.1). To evaluate the performance of the cell, three characteristics have been considered: i-v curve (also called polarization curve), already described in chapter 2, fig. 2.3, voltage curve, from which the degradation rate can be figured out, and finally Electrochemical Impedance Spectroscopy (EIS), which allows calculating both the series and polarization resistance, respectively  $R_s$  and  $R_p$ . EIS will be introduced in a next sub-sections. Data analysis were done using Ravdav, from [25].

### 4.1.1 Description of the test rig

The complete set up of the rig is reported in the following sketch:

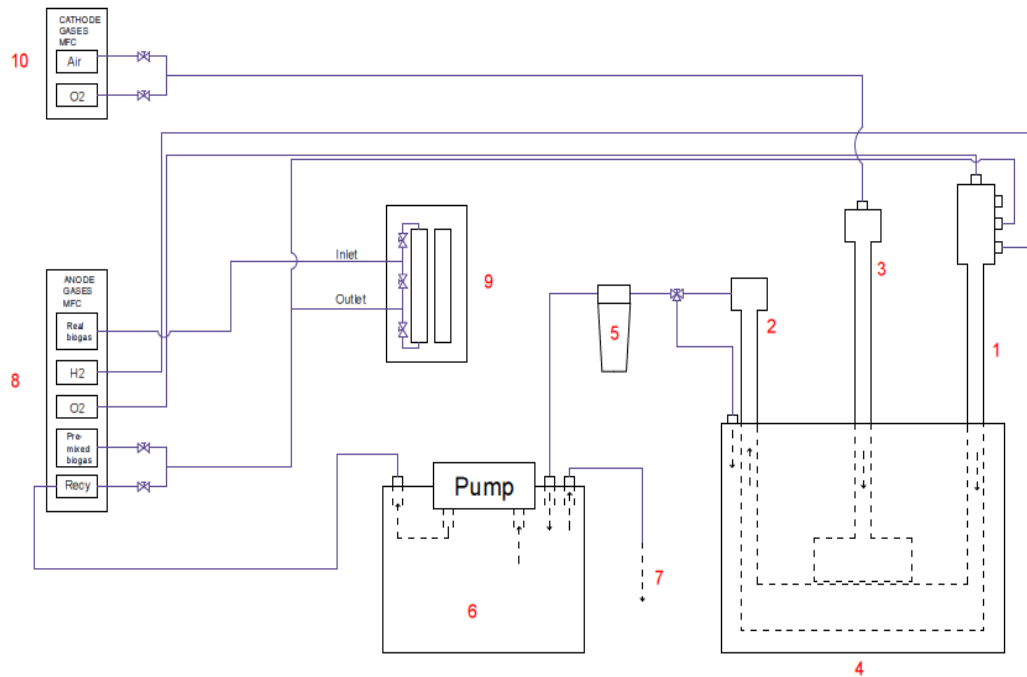


**Figure 4.1: Rig 5 set up, with exhaust recycling, biogas and particle filters**

- 1) Cell house inlet; 2) Cell house outlet; 3) Cathode inlet; 4) Furnace; 5) Particles filter; 6) Tank of the pump; 7) Exhaust rig; 8) MV and MFC anode board; 9) Activated carbon filter; 10) MV and MFC cathode board;

The gases from the anode MFC (8) flow through the anode inlet (1) and go inside the furnace (4). At the same time, the air/oxygen from the cathode side (9) flows through the cathode inlet (3) and inside the furnace, where they react with the other gases. Exiting then from the anode outlet (2), they pass through a particle filter (5) in order to remove potential undesired particles, especially of carbon, which can be formed due to the lower temperature of those pipes, before entering in the pump (6). Here the gases are sent again to the anode recirculation MFC (8). An activated carbon filter (9) (actually two, a principal one and a backup one) is also used, which has the goal of taking out the impurities, in case the cell house is fed with real biogas,

especially sulphur, which damages the cell blocking the pores of the anode. Activated carbon filter has been activated for the last experiment (test 8), in which real biogas has been used. When recirculation is not applied, the anode off-gases are simply put into the furnace and burnt, forming  $CO_2$  and  $H_2O$ , through a three-way valve and the pump is turned off. The flows of gases are controlled by MFC, through an online software, with also the presence of manual valves in order to cut-off the gas in case of emergency.

**Fuel cell** : The cells used for the experimental part were anode supported one, with a nominal surface area of  $16\text{ cm}^2$  and square shape ( $4 \times 4\text{ cm}$ ). As regards the material of the cell, they are resumed in the following table:

Layer	Material
Fuel Electrode	Ni/YSZ
Electrolyte	YSZ
Oxygen Electrode	LSC
Barrier Layer	CGO

Table 4.1: SoA anode supported cell materials

Yttria Stabilized Zirconia (YSZ) is used both for the electrolyte and the anode electrode, but some Nickel is also added to the anode in order to create the conductive phase. On the cathode side, a cerium gadolinium oxide (CGO) is followed by a LSC-CGO, where LSC stays for Lanthanum, Strontium, Cobalt, while the current collection layer is in LSM, where Cobalt is substituted by Manganese. An image of the cell after the first experiment (recirculation of 50% with pre-mixed landfill biogas) is reported in fig.4.2:

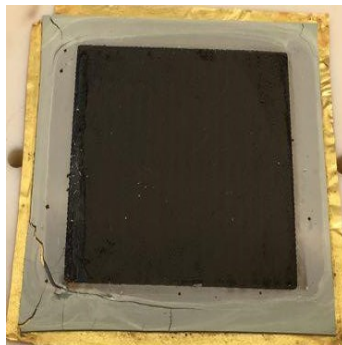
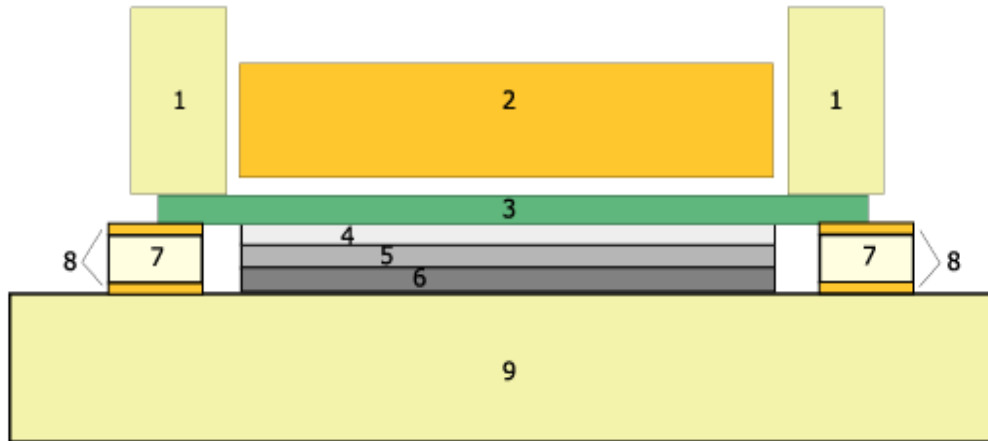


**Figure 4.2: Image of the cathode side of the cell after test, including the gold sealing**

**Cell house** : The cell needs to be feed with fuel gases at the anode and air/oxygen at the cathode, so a cell house has been used to achieve that without mixing the different flows. In the following picture a section of it is represented:



- |   |  |
|---|--|
| 1 Al <sub>2</sub> O <sub>3</sub> cell house - top                             | 6 Anode current collector (Ni plate)               |
| 2 Cathode current collector (Au mesh on Al <sub>2</sub> O <sub>3</sub> block) | 7 Al <sub>2</sub> O <sub>3</sub> sealing           |
| 3 Fuel cell   | 8 Au sealing                                       |
| 4 Anode current collector (Ni mesh, fine)                                     | 9 Al <sub>2</sub> O <sub>3</sub> cell house bottom |
| 5 Anode current collector (Ni mesh, rough, corrugated)                        |  |

**Figure 4.3: Cell house section (from [26])**

It is made of alumina (9)( $Al_2O_3$ ), a ceramic material able to resist to very high temperature. A Nickel plate of 0.1 mm thickness (6) is inserted in between in order to achieve a better electric conduction, as well as two Ni-mesh, the first one (5) with a thickness of 0.22 mm, while the second one is corrugated and reaches 0.7 mm (4). Above of these, the cell is placed (3) and a gold sealing is put around (8). Finally, an alumina support (1) is set in order to keep the cell fixed and the cathode is then located inside it (figure 4.3). The cathode part consists in a gold (Au) mesh on an alumina block, connected to another alumina pipe used to deliver the cathode gas (usually air, but also pure  $O_2$ ), as can be seen in figure 4.4.

In the picture (4.4) the cell house is shown. It is possible to individuate the anode inlet tube on the right and the outlet on the left. The red and blue cables are used to record temperature data, due to two thermocouples installed inside the big alumina tubes, while the transparent pipes are part of the  $p_{O_2in}$  and  $p_{O_2out}$  sensors, which measure the voltage on the anode and

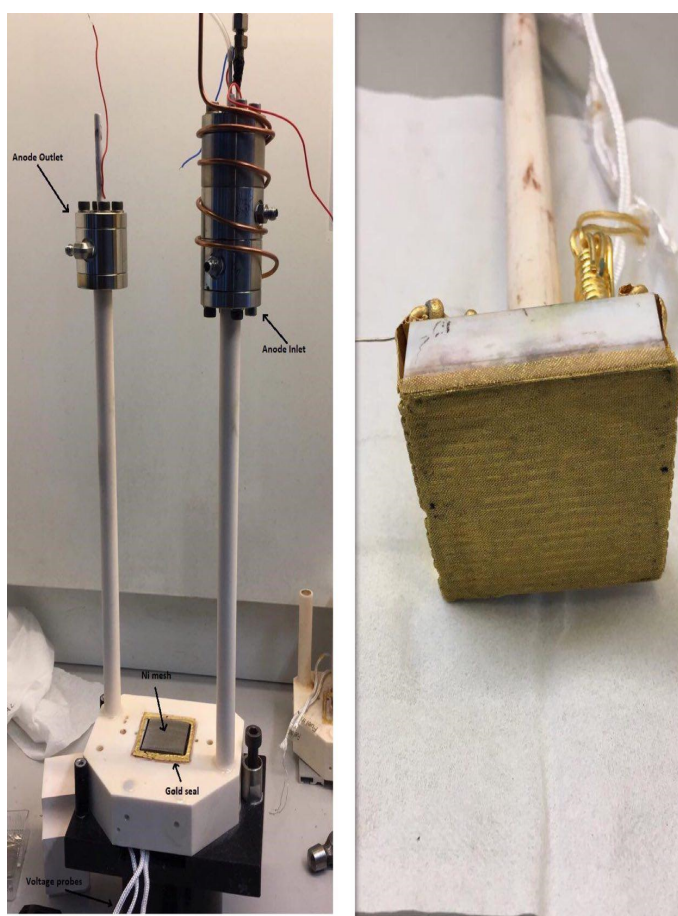


**Figure 4.4:** Anode part (left) and cathode part (right) of the cell house

cathode side. Finally, in the bottom part of the figure, there are the four platinum wires for the collection of the voltage.

**Pump** : Owing to the fact that gases arrive with a certain pressure at the inlet of the cell house, higher than the atmospheric one, it is not possible to directly recirculate the flow exiting from the cell just connecting the pipe again to the anode. For this set up, an axial pump has been used, with a relative pressure of 0.5-0.6 barg, indicated by a manometer on the top of it. As can be seen in fig. 4.1, the equipment consists of a tank, with a volume of approximately 7.5 liters, where the gases coming from the anode outlet are going. From there, they are sucking from the pump and sent in the recirculation branch. Everything is tight with screws and rubber seal in order not to have any leakages. On the top of the tank a control system

has been placed, which allows varying the speed, and, as a consequence, the pressure of the pump, number of rotation and current to the pump.

### 4.1.2 Cell start up and fingerprint

Every time the cell has to be substituted, the following start up procedure has been applied: firstly the cell house has to be placed inside a furnace, inside the ventilated cabinet, connecting then all the gas pipes and voltage/current wires, and heating everything up to  $850^{\circ}\text{C}$ , with a heating rate of  $1^{\circ}\text{C}/\text{min}$ . During the heating up process, the anode side is fed with argon (Ar), while the cathode with air. After that, the anode part of the cell needs to be reduced, passing from nickel oxide, recognizable due to the green color, to Ni, gray, as can be seen in fig. 4.2. To do it, the cell has been fed for 2 hours with a mixture of 9% of  $\text{H}_2$  in  $\text{N}_2$ , stopping meanwhile the Ar flow. Finally, gas can be switched to pure hydrogen, starting with 10 L/h and increasing it up to 25 L/h, while the flow of air at the cathode side is slowly increased up to 140 L/h. The cell is now ready for the so called fingerprint, which is a test of gas leaks and performance, done at different temperature and gas composition. The temperature variations are four in total, starting from  $850^{\circ}\text{C}$  and going down to  $700^{\circ}\text{C}$  in  $50^{\circ}\text{C}$  steps. For each temperature, six tests are done, with different percentage of  $\text{H}_2\text{O}$  at the anode, from 4p to 20p and 50p, and air or pure  $\text{O}_2$  at the cathode. Impedance spectra, as well as iv curve, were recorded for each step. In total, two cells have been used. A single cell has been used for more than one test, since the duration of a single experiment is about 150-160 h, so after each one, another fingerprint has been done, to evaluate the performance before and after, but limited to the case of  $750^{\circ}\text{C}$ , which is the temperature used for the investigation. Each test has been carried out in the same rig, equipped with a furnace, in which the cell house is put, gas supply with thermal mass flow controller (MFC), an electronic load and a very complex safety system (Safety Box) to control the gases. Temperature, gas flows and current were controlled through an online software, as also the electrochemical measures for the analysis.

### 4.1.3 Impedance spectroscopy: definition and characteristics

In order to better understand the degradation of the cell and to separate the various contributions, a useful instrument to use is electrochemical impedance spectroscopy (EIS). As explained by Njodzefon [27], a direct current bias through the system under investigation is superimposed with a sinusoidal signal  $i(t) = i_0 \sin(\omega t)$  of small amplitude  $i_0$ , where  $\omega = 2\pi f$  is the angular frequency, the corresponding sinusoidal voltage is recorded and the complex impedance  $Z(\omega)$  is calculated as the ratio of voltage and current, as follow:

$$Z(\omega) = \frac{u(t)}{i(t)} = Z' + jZ'' \quad (4.1)$$

where  $Z'$  is also called real part or Re or  $Z_{real}$ , while  $Z''$  is the imaginary part or Im or  $Z_{imag}$ . If the excitation signal is the current, the response is called galvanostatic EIS, while if the excitation signal is the voltage, is called potentiostatic EIS. Another important parameter is the distribution of relaxation time (DRT), which is a valuable pre-identification method that separates the polarization processes with different time constants directly from the impedance data. The DRT method uses the fact that every impedance can be represented as a differential sum of infinitesimal small RC-elements; for further information can be found in the literature ([27–29]). Dynamic processes in an electrochemical system have different relaxation times (RT), so the recording of an impedance spectrum is done for a certain number of frequencies, in a frequency range  $10MHz - 10mHz$  in this case. Processes with very short RT will be triggered at high f, while slower processes with longer RT are triggered at low f.

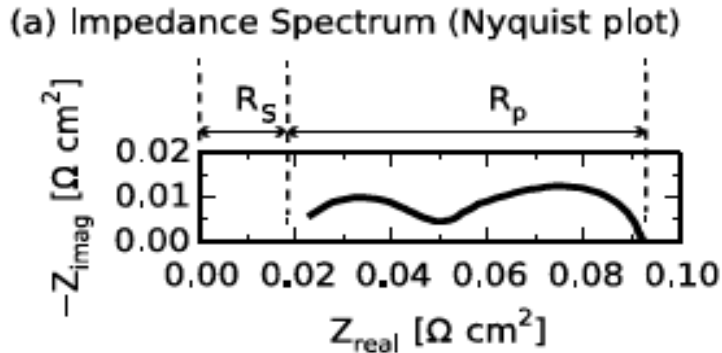


Figure 4.5: Nyquist plot (from [27])

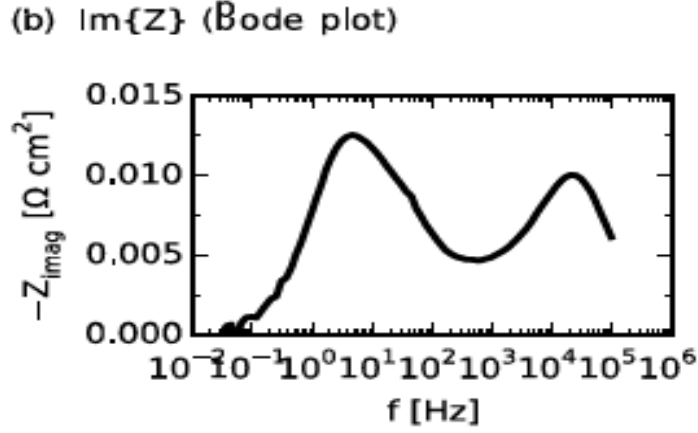


Figure 4.6: Bode plot (from [27])

The impedance response can be illustrated in different ways, as for example the Nyquist plot or Bode plot as shown in figure 4.5 and 4.6. In the first one (4.5) the resistances are illustrated:  $R_s$  is the series resistance, while  $R_p$  is the polarization resistance. More information can be analysed plotting the imaginary part of the impedance as a function of frequency (Bode plot, 4.6) and, moreover, small changes of the various contributions can be evaluated using the difference of these spectra, plotting it as a function of frequency, for example as done by Hagen et al. [30]. Impedance can also be represented by an equivalent circuit. From the definition of basic circuit elements and their behaviour in AC voltage, their impedance written in complex numbers can easily be derived, and are given in table 4.2.

Element	Impedance
Resistance R	R
Capacitance C	$\frac{1}{j\omega C}$
Inductance L	$j\omega L$
Constant Phase Element CPE	$\frac{1}{Q_0(j\omega)^n}$

Table 4.2: Basic circuit elements impedance (from [26])

Two different approaches can be used in the fitting of SOFC impedance spectra. If a detailed knowledge of the individual processes is not required, a simple equivalent circuit modeling the shape of the impedance spectrum only is sufficient: a resistor for ohmic resistance in series with two elements of a CPE and a resistor in parallel each (see [31]). These two R-CPE elements

model the sum of low and high frequency processes, from which the contributions due to mass transport phenomena (low  $f$ ) and from charge transfer (high  $f$ ) can be evaluated. The number of processes depends both on cell and gases composition. Finally, in table 4.3 the different anode processes with respect to the frequency are reported for the cell type used in this work, underlining also the key factors which intervene in the processes themselves.

<b>Frequency Range [Hz]</b>	<b>Related Processes</b>	<b>Key Factors</b>
35000-20000	Ionic transport in ceramic matrix	Temperature
4500-500	Charge transfer B at Ni-YSZ TP	Temperature, $p_{H_2}$
100-10	Gas diffusion in anode support/gas channels	$p_{H_2}$ , $p_{O_2}$ , micro-structure
5-0.1	Gas conversion/diffusion /reforming reactions	$p_{H_2}$ , $p_{H_2}$ , ratio C/H/O in fuel

Table 4.3: Anode polarization processes and key factors with respect to frequency in impedance spectra for a SOFC cell consisting of Ni-YSZ (from [30])

#### 4.1.4 Biogas anode fuel recycling study: test

The composition for the various experiments changes, according to tab. 2.1. In the case of landfill biogas, the first test (called test 0) which has been carried out is the one with extra  $CO_2$ , in order to have a comparison between recirculation and extra reforming agent effect. Eight experiments have been carried out: the first four adding simulated exhausts fuel via the MFC, according to the simulation (see section 3.2), called pre-mixed recirculation, the second four using a pump to recirculate (as illustrated in 4.1). The settings are shown in table 4.4 and 4.5.

Test nr.	Biogas	RR [%]	$CH_4$ [%]	$CO_2$ [%]	$N_2$ [%]	$H_2O$ [%]	i [ $A/cm^2$ ]	Duration [h]
0	Landfill	0	23	48	29	0	0.5	360
1	Landfill	50	24.9	24.5	38.3	9.1	0.5	150
2	Landfill	30	28	24.2	39.9	6.4	0.5	150
3	Wastewater	50	46.9	35.2	0.78	13.3	0.92	150
4	Wastewater	30	52.7	35.4	0.54	9.5	0.92	150

Table 4.4: Pre-mixed biogas experiments overview with pre-mixed recirculation

For landfill, the other gases are negligible, while for the waste water there is also a small percentage of  $CO$  and  $H_2$ , respectively around 1.5% and 2.3% with high RR and around 0.8% and 1% for the low RR.

For the second four tests, three are performed with pre-mixed biogas, landfill composition, using a pump to recirculate the anode exhaust, while in the fourth one real landfill biogas is used, filtered before entering the cell, with an activated carbon filter, in order to eliminate impurities. In particular, test 7 (RR = 0.1) has to be performed using the pump, since the amount of certain gases recirculated was too low for the MFC to be done with the pre-mixed recirculation. The other three cases, instead, were carried out in order to understand the differences, if present, between the pre-mixed recirculation and recirculation through the pump.

Test nr.	Biogas	RR [%]	i [A/cm <sup>2</sup> ]	Duration [h]
5	Pre-mixed Landfill	50	0.5	600
6	Pre-mixed Landfill	30	0.5	150
7	Pre-mixed Landfill	10	0.5	150
8	Real Biogas	30	0.5	150

Table 4.5: Pre-mixed and real biogas experiments using pump to recirculate

## 4.2 Results of tests study

In this section the results from the laboratory tests will be analyzed, making use of data collected during the hours of experiment and calculating the degradation of the cell also through formula such as 4.2, used to understand the voltage decreasing in percentage.

$$D_r = \frac{m}{u_{start}} * 1000h \quad (4.2)$$

where  $m$  is the slope of the voltage, identified by the straight line equation  $y = mx + q$ , and  $u_{start}$  is the voltage of the cell at the beginning of the test; everything is then multiplied for 1000 hours, in order to standardize all the experiments and have a comparison with other data available in literature. Other parameters that allow evaluating degradation and changes in the cell are the polarization resistance ( $R_p$ ) and the ASR, which are correlated by the formula:

$$ASR = R_p + R_s \quad (4.3)$$

where  $R_s$  is the series resistance, caused by the wires used to measure voltage and current density. The two resistances can be evaluated looking at the impedance spectra, as illustrated in section 4.1. Regarding ASR, it can be calculated using the following formula (from [30]):

$$ASR = \frac{(OCV - V_i)}{i} \quad (4.4)$$

where OCV is the voltage at open circuit,  $V_i$  is the voltage under current during the test and  $i$  is the current density. As done with the degradation rate, the ASR increment has been extended to 1000 h, since the experiment time was just 150 h, simply through a proportion:

$$ASR_{1000h} = ASR_{150h} \cdot \frac{1000h}{150h} \quad (4.5)$$

### 4.2.1 Landfill: pre-mixed biogas

The first composition which has been analyzed in test 1 and 2 is fundamentally the same of the landfill gas, with the advantages that it is re-created directly in the rig and so it does not contains any impurities, avoiding cell damaging. This means that an activated carbon filter is not needed. According to the theoretical simulations, the first investigation has been done using a current density of  $0.5 \text{ A/cm}^2$ , which assures a FU of 0.6.

Test nr	$u_{start}$ [V]	$\frac{D_r}{1000h}$ [%]	$R_p$ [ $\Omega \cdot \text{cm}^2$ ]		$R_s$ [ $\Omega \cdot \text{cm}^2$ ]		ASR [ $\Omega \cdot \text{cm}^2$ ]	
			before	after	before	after	before	after
0	0.809	1.112	0.275	0.275	0.180	0.189	0.401	0.409
1	0.808	3.711	0.36	0.38	0.181	0.181	0.464	0.472
2	0.816	3.675	0.3408	0.3491	0.179	0.180	0.452	0.458

Table 4.6: Landfill: experiments with pre-mixed recirculation

**Test 0** : The first test that has been carried out was the so called reference test since the cell has been fed with the landfill composition pre-mixed biogas, but constantly with the 2 L/h of extra  $CO_2$ . Even if the experiments last for 360 hours, there is not an increment in the polarization resistance and the degradation rate is only 1% in 1000 h, as can be seen from table 4.6. On the other hand, looking at the area of specific resistance, there was an increment of more than 5% in 1000 h, illustrated in fig. 4.7. Each following test will then compared to this one, in order to understand the advantages of recirculation. Voltage, power and efficiency are illustrated in tab. 4.7.

Average voltage [V]	$P_{el}$ [W]	$\eta_{el}$
0.806	6.44	0.47

Table 4.7: Test 0: average voltage, power and efficiency without recirculation

The average voltage, and, therefore, power density and efficiency are so high due to the fact that this was the first experiment, so the cell was new and had better performance.

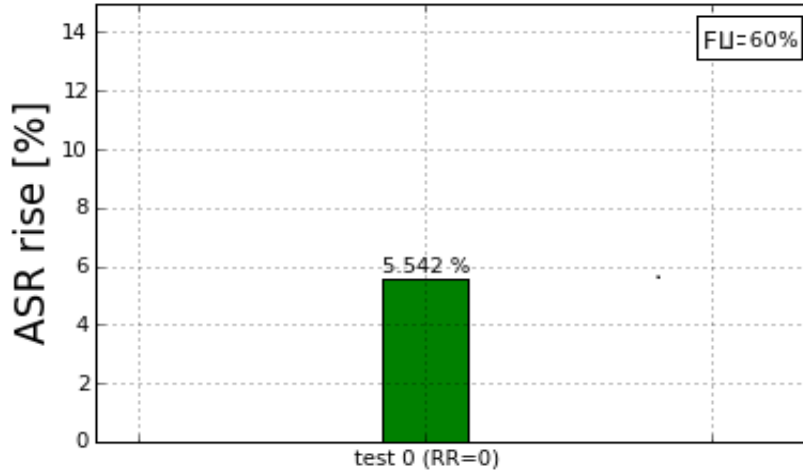


Figure 4.7: ASR percentage increment in 1000 h with extra  $CO_2$

**Test 1** : As starting point, it has been chosen to recirculate 50% of the anode off-gas, so 2 L/h. The total flow does not change, since 2 L/h of extra  $CO_2$  has simply been taken out and substituted by the recirculation flow. The first data to be analyzed was the cell voltage, from which it is possible to evaluate the degradation rate of the cell (reported in tab. 4.6): it amounts of approximately 4% in 1000 h of test. It is clear (fig. 4.10, a)) that the voltage declines quite fast under this condition, due to the high percentage of steam, which, on one hand, allows not having problem of carbon deposition, but on the other, it damages the cell quite a lot (as studied by ??). The points in which the line presents some disturbances are caused by the impedance measurements, but they do not influence the results. Other parameters which are interesting to analyze are the resistances, polarization  $R_p$  and series  $R_s$ , which can be figured out through the study of the impedance before and after the test.  $R_s$  was stable, while the increment of polarization resistance is more pronounced, due to the high amount of steam produced and recirculated in the cell. This rise has been reported in table 4.6. Moreover, fig. 4.9 (a) illustrates the delta of the Bode plot, obtained simply subtracting the graph after the test to the one before the test, both calculated at OCV. The red line represents the test under consideration. It can be seen that there is an increment of the impedance both in the range 0.01-0.1 Hz, a small increase, which is related to mass transfer, and in the  $10^2$ - $10^3$  Hz one, a quite big rise, in the area related to charge transfer. The polarization resistance growth of  $0.02 \Omega \cdot cm^2$ , a value which is quite high with respect to test 0, where it remained approximately constant. Finally, the last plot is the i-v curve and the power voltage curve for the cell (fig. 4.8, a)), even in this case evaluated before and

after the test. In these graphs is really difficult to catch the difference between the curves before and after the test, since it is negligible, due to the fact that 150 h of test are not sufficient to cause huge changes. This is also confirmed by the increment of the area of specific resistance, equal to approximately 11%; the value is high because it is calculated in 1000 h, as illustrated in fig. 4.9, b). Owing to the fact that the high degradation behaviour is caused by a large amount of water recirculated, the choice was to reduce the RR, seeing if it leads to better performance (as found out in simulations) and lower degradation, more similar to test 0 one, so 5-6%. Regarding voltage and efficiency, they have been evaluated from data analysis and through calculation, using (2.24): the initial voltage is slightly higher, as well as the power, but with an increment which is negligible, not in accordance to what was expected. The reasons are the not perfect composition of the recirculation flow since some value of gas had to be rounded in order to respect the cut-off flow of MFCs. In addition, the cell at that point had run for thousand hours, so the performances were a bit affected by degradation. Everything is resumed in tab. 4.8.

Average voltage [V]	$P_{el}$ [W]	$\eta_{el}$
0.8067	6.45	0.47

Table 4.8: Test 1: average voltage, power and efficiency with recirculation of 50%

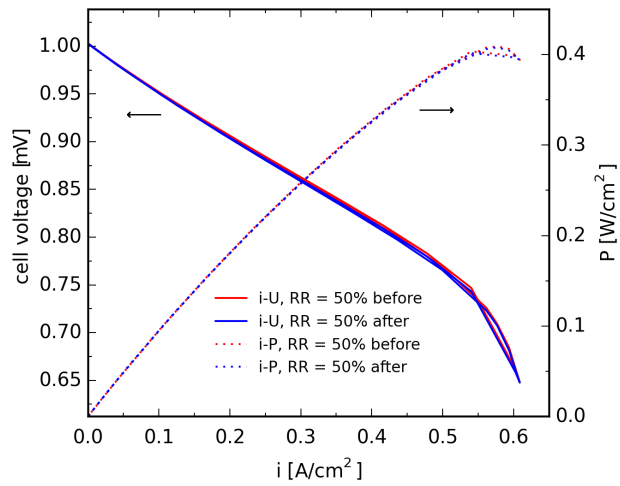
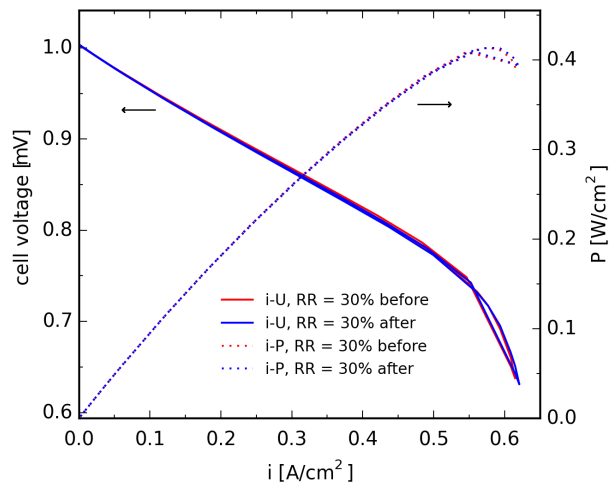
**Test 2** : For the second test, the rate of recirculation has been decreased to 30%, as done previously in the simulations. Only 1.2 L/h has been recirculated, so the total flow decreased from 6 to 5.2 L/h. The voltage results to be higher with respect to the previous test (fig. 4.10, b) according to the Nernst equation (2.13), due to the fact that fuel is less diluted, so the partial pressure of the methane is higher and therefore the OCV. Regarding the degradation rate, evaluable through an analysis of the voltage, it is similar to test 1, with a negligible difference (1 % less). Having a look to fig. 4.9 (a), it is interesting to note that the delta of the Bode plot, in this case, is negative in the mass transfer region (range 0.01-0.1 Hz), while in the high frequency one it still increases, commensurate with the previous case, since the difference between the two peaks is not so pronounced. The most appealing data is the polarization resistance, calculated in tab. 4.6: the resistance rose approximately of  $0.01 \Omega \cdot cm^2$ , so less than the half with respect to the 50 % recirculation case. This could be caused by the fact that 3 % less water

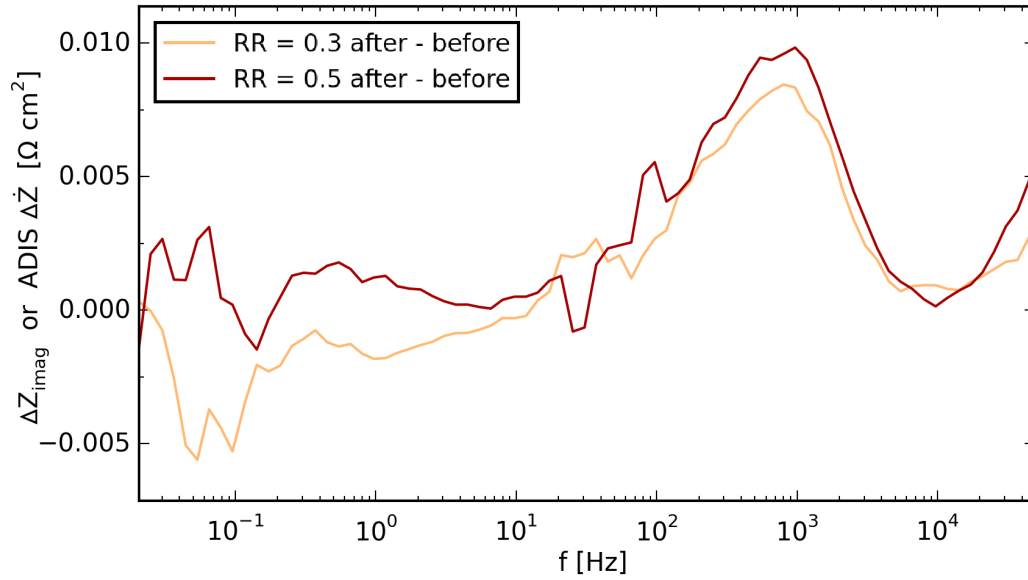
is recirculated, leading to a lower degradation. In figure 4.8 are shown the i-U curves before and after the test, which result in no significant differences, even less with respect to the previous test, and confirmed by the percentage rise of the ASR in 1000 h, equal to approximately 9% (4.9, b)). As regards the electric power and efficiency, there is an increase with respect to test 1, only related to the rise of voltage, since the current and the volumetric flows of fuel are unvaried. The electric efficiency value is with 48% close to 50%, so more than 2% higher with respect to test 0.

Average voltage [V]	$P_{el}$ [W]	$\eta_{el}$
0.8134	6.50	0.48

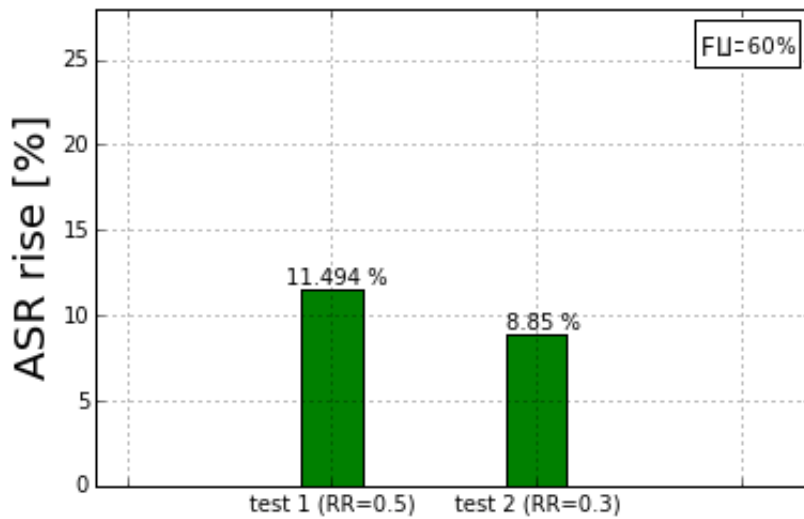
Table 4.9: Test 2: average voltage, power and efficiency with recirculation of 30%

Unfortunately, tests with only 10% of recirculation could not be done due to the fact that the volumetric flows of the anode exhausts in those conditions were too low for the MFC, which have a minimum cut-set imposed.

(a) *i-U* curve, pre-mixed landfill  $RR = 50\%$ .(b) *i-U* curve, pre-mixed landfill  $RR = 30\%$ .Figure 4.8: *i-U* curves from test 1 and test 2

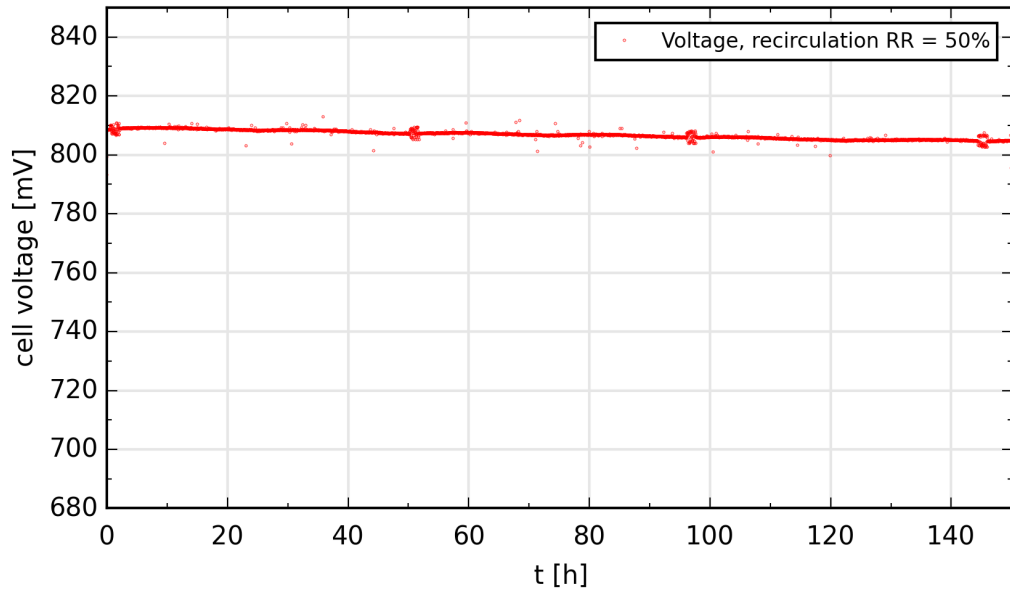


(a) Delta Bode plot for pre-mixed recirculation applied to landfill pre-mixed biogas.

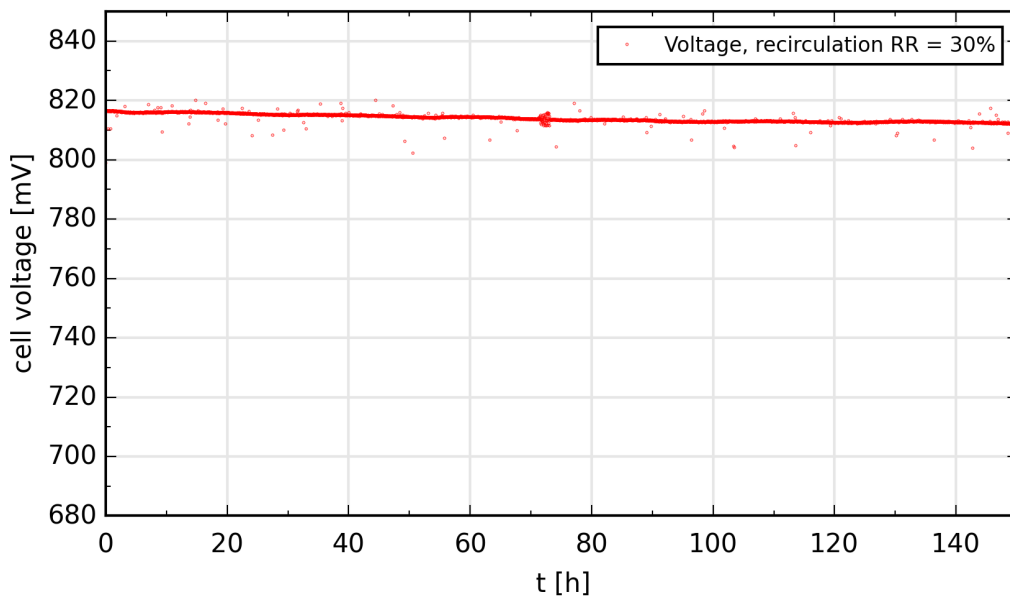


(b) ASR percentage increment in 1000 h, pre-mixed landfill.

Figure 4.9: Experimental data from test 1 and test 2



(a) Voltage over time, pre-mixed landfill RR = 50%.



(b) Voltage over time, pre-mixed landfill RR = 30%.

Figure 4.10: Voltage evolution from test 1 and test 2

### 4.2.2 Waste Water: pre-mixed biogas

The second composition analyzed is instead the one of a typical waste water biogas, with a higher amount of methane and carbon dioxide, and a smaller one of nitrogen with respect to landfill. The higher amount of  $CH_4$  allows using a bigger current density, which defines also the FU. Operational condition is  $0.92 A/cm^2$  for the current density, which means  $FU = 0.6$ . Owing to the fact that the amount of nitrogen was very low, the MFC was not able to guarantee it and so it has been neglected: the initial composition was 57% of  $CO_2$  and 43% of  $CH_4$ .

Test nr	$u_{start}$ [V]	$\frac{D_r}{1000h}$ [%]	$R_p$ [ $\Omega \cdot cm^2$ ]		$R_s$ [ $\Omega \cdot cm^2$ ]		ASR [ $\Omega \cdot cm^2$ ]	
			before	after	before	after	before	after
3	0.700	5.713	0.5755	5899	0.177	0.182	0.385	0.394
4	0.708	4.236	0.4712	0.5517	0.177	0.181	0.385	0.387

Table 4.10: Waste water: experiments without pump

**Test 3** : Even in this case the analysis started from the higher value of recirculation,  $RR = 50\%$ . Regarding the voltage, the degradation rate is approximately 6 %, so 55% higher in comparison to landfill one (tab. 4.10), due to the gas composition, which requires an higher value of current density: not only the current causes degradation, but also it leads to a bigger production of steam. With this composition, also some CO is recirculated, but the amount is so low that it does not influence the equilibrium reactions inside the cell and therefore it has been considered negligible. It is interesting to note that the higher decrease of cell voltage happens in the first 50-60 hours (fig. 4.13, a)), while after the trend is more stable. As regards the polarization resistance,  $R_p$  (tab. 4.10), surprisingly the increment is quite low (tab. 4.10), equal to approximately  $0.015 \Omega \cdot cm^2$ , which is close to the one of test 2 (landfill,  $RR = 30\%$ ). This unusual result can be explained looking at tab. 4.4, where the percentage of steam, and so its partial pressure, is reported: it amounts to 9%, so the partial pressure is lower than the previous case with landfill. The delta Bode plot (fig. 4.12, a)) shows a quite stable behaviour around zero, with only a small variation for low frequencies, negative around 0.01 Hz and positive for 0.1 Hz, while a more significant deviation is visible in the charge transfer region ( $10^2$ - $10^3$  Hz). Finally, having a look to the i-U curve before and after the test, it is clear that there is a small decrease in the maximum current density, equal to  $0.02 A/cm^2$ , higher with respect to landfill case (fig. 4.11, a)). Directly connected with the i-U curve there is

the ASR, which increases of approximately 16% in 1000 h, as shown in fig. 4.12, b), value 1.35 time higher than the respective test with landfill composition, confirming the fact that the cell is more stressed using waste water biogas. Regarding power and efficiency, everything is reported in tab. 4.11: as expected, due to the higher current density (see 3.4), the ohmic losses are higher, leading to a lower value of the voltage, according to 2.15; this impact negatively on the power and on the efficiency, which results to be 17% lower with respect to the landfill case.

Average voltage [V]	$P_{el}$ [W]	$\eta_{el}$
0.695	10.23	0.402

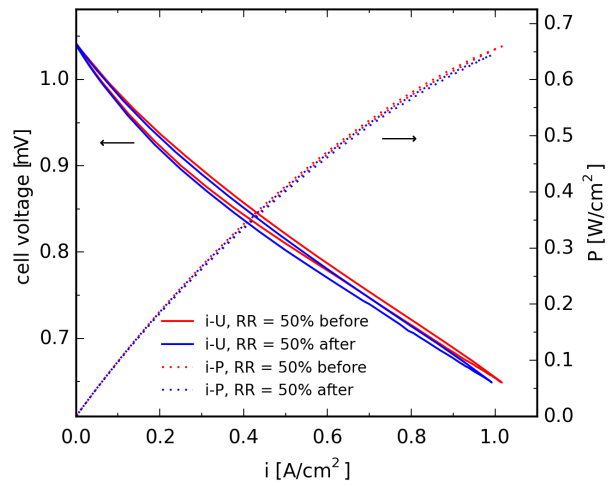
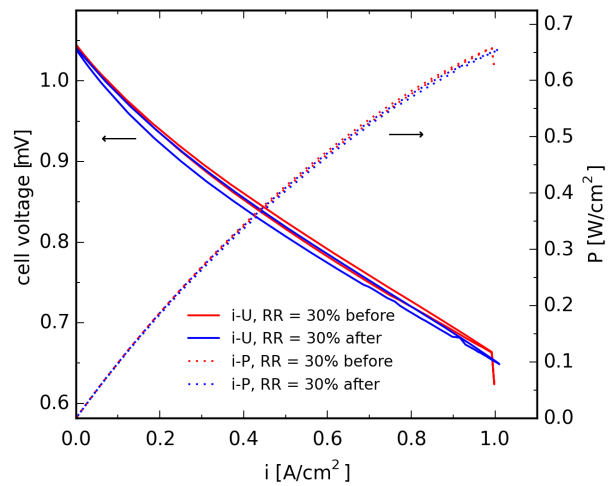
Table 4.11: Test 3: average voltage, power and efficiency with recirculation of 50%

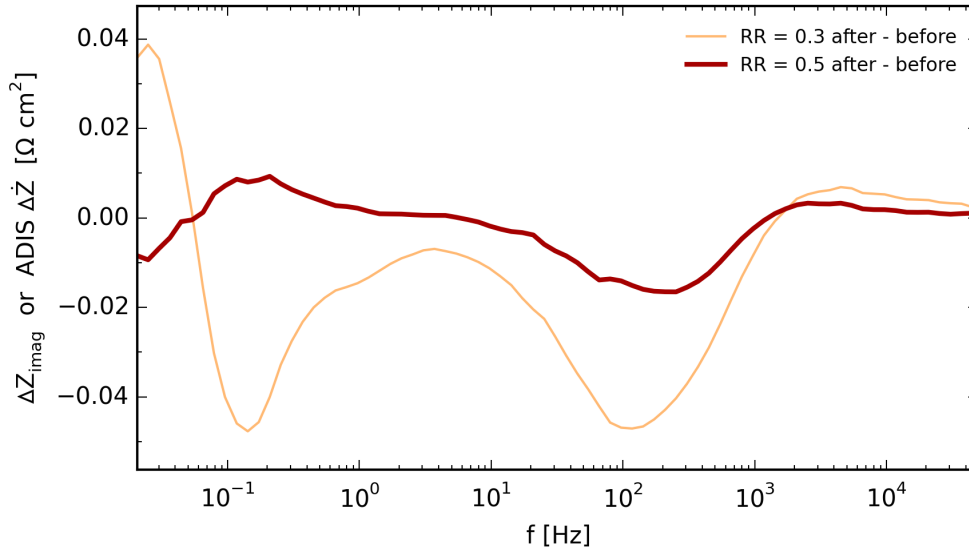
**Test 4** : As proved during the simulation study (chapter 3, fig. 3.6) it is possible to decrease the recirculation ratio and not having the problem with carbon formation, so it has been decided to run the cell with RR = 30%. Similarly to the other wastewater test, the voltage has a quite high decrease, especially in the first part of the experiments (40 hour), even more pronounced than the 50% recirculation one, becoming then more stable in the last part (fig. 4.13), with a total degradation rate around 4% in 1000 h, as reported in tab. 4.10. This high degradation rate is a merge of high current density and water content to the cell. The most appealing parameter in this test is the impedance analysis, in which even though  $R_s$  essentially does not change, as expected, the polarization resistance has a very high increment of  $0.08 \Omega \cdot cm^2$ , illustrated in tab. 4.10. That rise is almost 8 times bigger than test 2, in which the same RR has been used, and 5 times than test 3, so a more deeply analysis has to be carried out in order to understand if that value is a mistake in the measurement or just an experimental data. One reason can be a higher leakage occurred. Extracting the cell, it did not present carbon formation, so that value is not imputable to carbon. According to the 4.12 b), also the delta Bode plot 4.12 a), present diffuse changing: it shows an increment in the very low frequencies region (0.01 Hz), while a rise in both low (0.1 Hz) and medium-high ( $10 - 10^2$  Hz), ending with a stable behaviour for very high f ( $10^3 - 10^4$  Hz). Different is the situation looking at the i-U curve (fig. 4.11, b), where a negligible decrement of maximum current density and power density has been observed, confirmed by the ASR percentage rise, which is surprisingly lower than 1%, so the half with respect to the other

tests, in contrast with the polarization value found before. Even in this case, power and efficiency have been calculated and reported in tab. 4.12: values are similar to the previous case, with an increment in the efficiency of 1%, but 19% lower with respect to the landfill case, in the same recirculation condition.

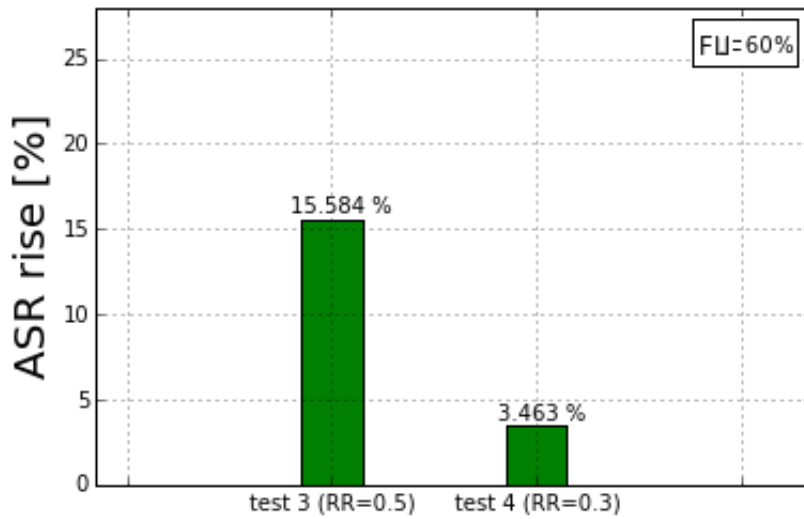
Average voltage [V]	$P_{el}$ [W]	$\eta_{el}$
0.700	10.304	0.405

Table 4.12: Test 4: average voltage, power and efficiency with recirculation of 30%

(a) *i-U* curve, pre-mixed waste water  $RR = 50\%$ .(b) *i-U* curve, pre-mixed waste water  $RR = 30\%$ .**Figure 4.11: *i-U* curves from test 3 and test 4**

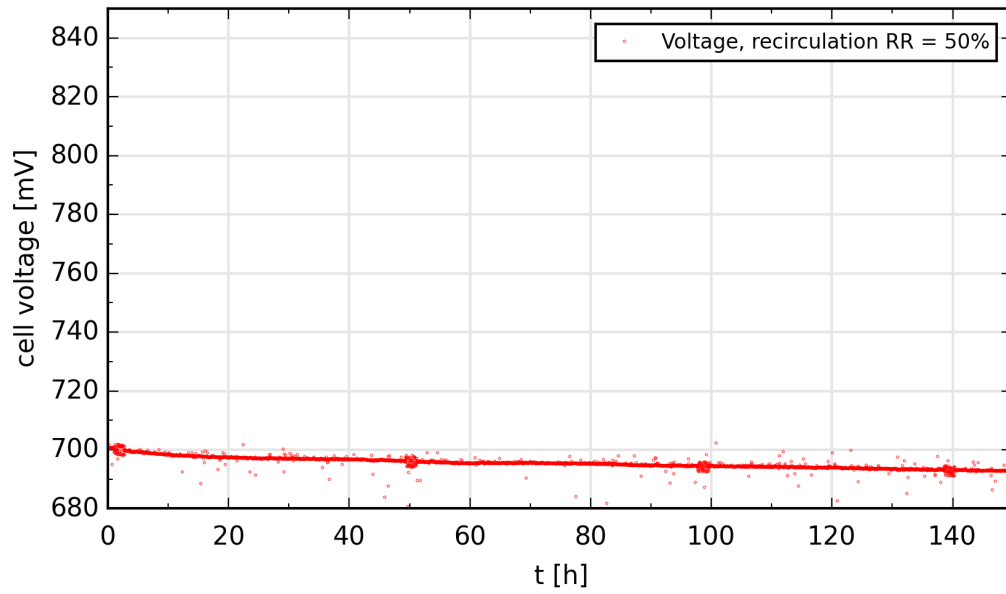


(a) Delta Bode plot for pre-mixed recirculation applied to waste water pre-mixed biogas.

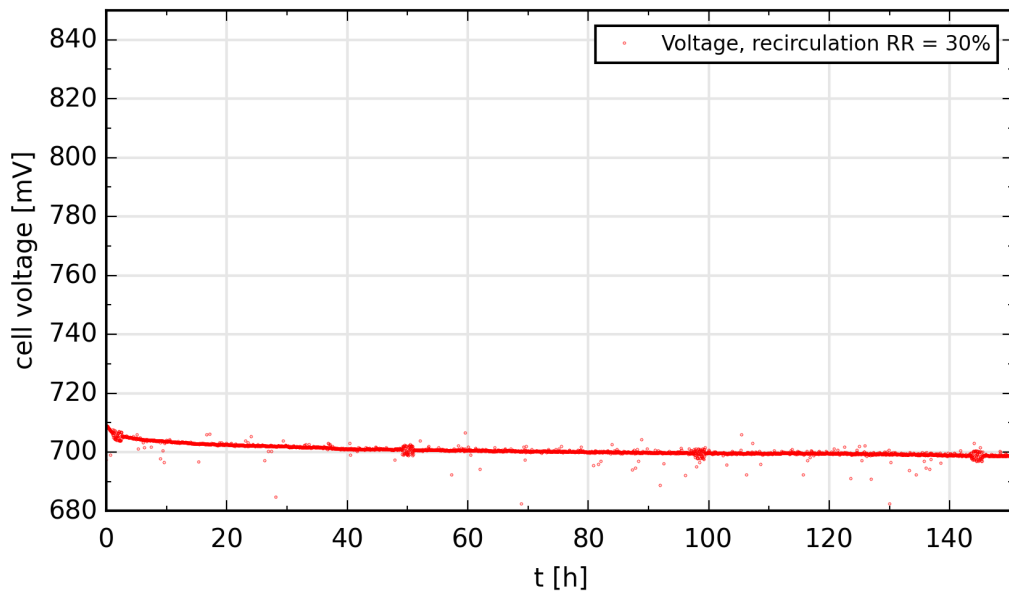


(b) ASR percentage increment in 1000 h, pre-mixed waste water.

Figure 4.12: Experimental data from test 3 and test 4



(a) Voltage over time, pre-mixed waste water RR = 50%.



(b) Voltage over time, pre-mixed waste water RR = 30%.

Figure 4.13: Voltage evolution from test 3 and test 4

### 4.2.3 Recirculation using pump: pre-mixed and real biogas

Finally, in order to have a better understanding of recirculation, four experiments have been carried out using a pump to move the gases, as described in section 4.1.1. The scheme of the system is reported in fig. 4.1, where the used pump is also shown. This part is divided into two sections: the first is dedicated again to the landfill pre-mixed gas, while the second one regards the real biogas, which includes also impurities to be purified before feeding the cell. Each experiment has been carried out using a current density of  $0.5 \text{ A/cm}^2$ , ensuring a fuel utilization of 60%. During these tests with the pump part of the water recirculated has been lost due to condensation into the particle filter and the pipes: it has then been measured, finding that the quantity is much less than 1% of the total in each experiment, so negligible.

Test nr	$u_{start}$ [V]	$\frac{D_r}{1000h}$ [%]	$R_p$ [ $\Omega \cdot \text{cm}^2$ ]		$R_s$ [ $\Omega \cdot \text{cm}^2$ ]		ASR [ $\Omega \cdot \text{cm}^2$ ]	
			before	after	before	after	before	after
5	0.809	8.646	0.2886	0.3978	0.184	0.196	0.42	0.511
6	0.803	7.467	0.3123	0.3219	0.174	0.179	0.431	0.444
7	0.774	5.169	0.4362	0.4470	0.175	0.185	0.495	0.508
8	0.776	11.596	0.4806	0.5014	0.185	0.186	0.483	0.501

Table 4.13: Landfill: experiments with pump

**Test 5** : In the first test using the pump a recirculation ratio of 50% has been considered, according to the previous sections. Only in this case, a long duration test has been performed (approximately 600 h), in order to understand the behaviour of the cell in a long term experiment. Owing to the fact that the MFCs are working at 0.5 bar, the pressure of the pump was set to that value, while the fuel recirculation MFC to 2 L/h. Since the pump has been used, there is a fluctuation in the recirculation flow related to the pressure fluctuation in the pump, which has an impact on the voltage, creating some instability with respect to the previously analyzed tests. In figure 4.14 has been illustrated the voltage decrease in 600 h, while, in order to compare the result with the next two test, in fig. 4.17 the voltage degradation in 150 h has been illustrated. In the first one, the voltage drop is constant, but analyzing in depth the second one, it is possible to recognize a lower degradation zone in the first 60-70 hours, while, after, the slope of the curve tends to rise. This is caused only by the high water content in

the recirculation branch, due to the chosen RR value, not by carbon particle eventually deposited on the anode, since the cell has been extracted after the test and did not present any traces of carbon deposition. Even in this case, the big fluctuations are deriving from the impedance analysis. The degradation rate is reported in tab. 4.13 and it is really high, approximately 9%, more than the double with respect to the same test did with 50% of recirculation, but without the pump (pre-mixed recirculation, test 1). Such a result was expected, since more variables have to be taken into account using a pump, but nonetheless surprisingly high. Through the impedance analysis also the polarization and series resistances have been evaluated and reported in tab. 4.13: the increment of  $R_p$  is really high,  $0.11 \Omega \cdot cm^2$  in 600 h (tab. 4.13), but in line with the test number 1.  $R_s$  also experienced an increase, but negligible. Regarding the delta Bode plot (fig. 4.15, a), although in the low frequency part the line is stable around 0 (mass transfer zone), in the high frequency part, representing the charge transfer zone, there is an increase of the curve, very similar to the one obtained in the previous test (4.9, a)). Finally, i-U curves before and after the 600 h have been examined, noticing a decrement of current density equal to  $0.3-0.4 A/cm^2$  and as well, a decrease of  $0.5 W/cm^2$  of power density, representing almost 10% of the total (4.16, a). Directly related to the i-U curve, the rise of the ASR is high as well, reported in figure 4.9, b), reaching almost 37%. As regards voltage, power and efficiency, they are resumed in tab. 4.14. These values are lower with respect to the one of test 0, the extra  $CO_2$  experiment, but this could be caused by the long operation time of the cell. The fact that after such amount of working hours under recirculation the efficiency is only 0.04 lower compared to the reference test 0 with  $CO_2$ , means that recirculation has a good impact on the cell.

Average voltage [V]	$P_{el}$ [W]	$\eta_{el}$
0.793	6.344	0.464

Table 4.14: Test 5: average voltage, power and efficiency with recirculation of 50%

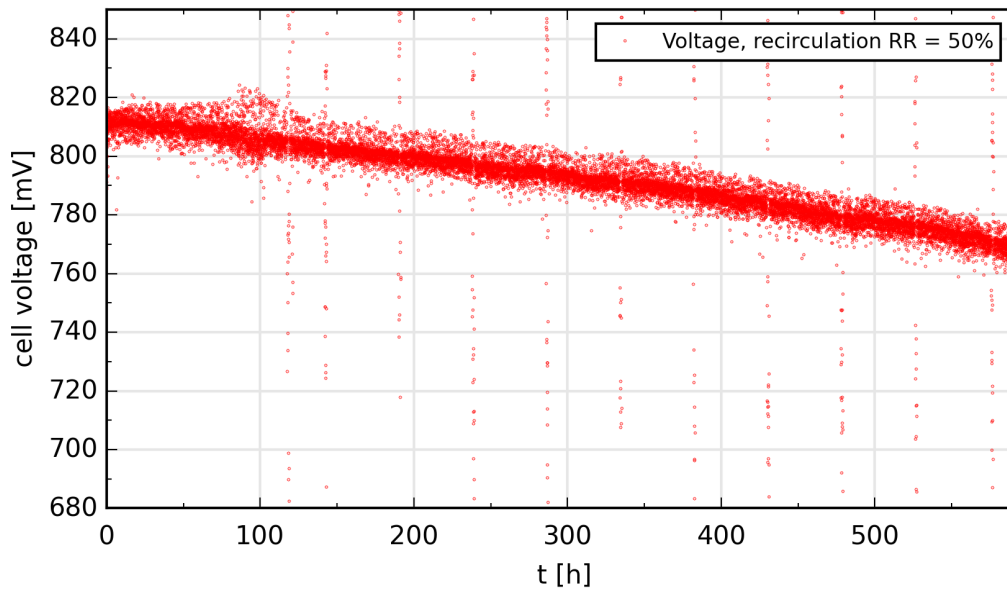


**Figure 4.14: Voltage over time, pre-mixed landfill RR = 50%, 600 h**

**Test 6** : Following the same order of before, the second test with the pump has been carried out using a RR = 30%. This test has been stopped after 140 hours, due to some problems occurred to the pump. That is also the reason why, looking at the voltage curve (see fig. 4.17, b)), in the last 20-25 hours the fluctuations result to be bigger than usual. The voltage drop was stable along the test (4.17, b)), with a degradation rate reported in tab. 4.13, still high, but almost two percentage point lower than test 5 (RR = 50%). The series resistance, substantially, does not change, while the polarization one slightly increases of  $0.01 \Omega \cdot cm^2$  in 140 h (tab. 4.13). The delta Bode graph (4.15, a)) shows a behaviour which is in opposition with respect to the test 2, since there is an increase of the curve in the low frequency area, while it significantly decreases in the high frequency one, so the most important change happened because of charge transfer and no more due to mass transfer. Looking at the i-U curves, no relevant changes occurred, in line with previous tests, because of the short testing time (4.16, b). Another interesting parameter is the ASR, which rise of approximately 21% (4.15, b)), which means the double with respect to test 2, confirming the higher degradation of these test in comparison to the pre-mixed recirculation ones. As expected, even in this case the voltage is higher with respect to the 50% recirculation experiment (1%) and, therefore, power density and efficiency are bigger, but still below the extra  $CO_2$  one, for the previously

mentioned reason.

Average voltage [V]	$P_{el}$ [W]	$\eta_{el}$
0.801	6.408	0.468

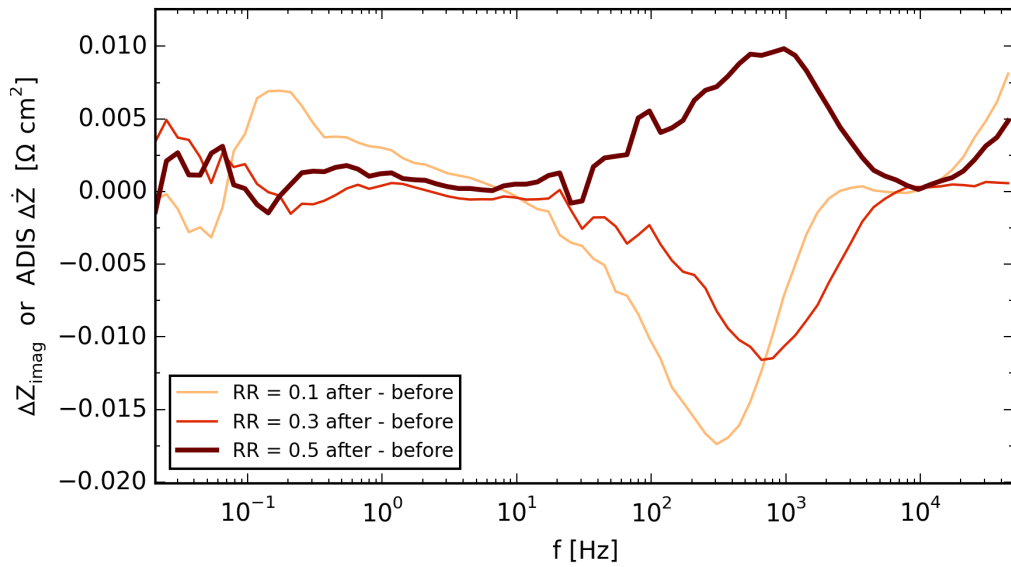
Table 4.15: Test 6: average voltage, power and efficiency with recirculation of 30%

**Test 7** : The last test using pre-mixed biogas has been carried out with a recirculation ratio of 10%. Due to the very low amount of recirculated gas, it was possible to perform it only with the pump, with a recirculated flow of 0.4 L/h. The expectations were a higher voltage and efficiency, due to the fact the fuel is not so diluted, but they were not completely met since the cell was operated already for approximately 1800 hours, so the performances were really worse than before. Moreover, this test was performed immediately after the waste water ones, which stressed the cell particularly. Even in this case, the test was stopped some hours before the 150 h initially planned, due to a technical error of the system. The voltage drop is stable and it presents some fluctuation, due to the pressure variation caused by the pump, with a degradation rate of 5%, shown in tab. 4.13 and lower than before: it is interesting to note that the less recirculation is applied, the more delta there is in the degradation rate, demonstrating again the tight correlation between degradation and water amount recirculated. Despite the fact that the degradation rate decreases quite a lot, this trend is not confirmed looking at the polarization resistance: the increment is  $0.01 \Omega \cdot cm^2$  in 140 h (tab. 4.13), so in line with the previous test. This is also confirmed by the delta Bode plot (4.15, a) which has a similar trend in the charge transfer zone ( $10^2 - 10^3 Hz$ ) with an decrease of the signal, while in the mass transfer zone ( $10^{-2} - 10^0 Hz$ ) and in the high frequency one ( $f > 10^4$ ) there is a more pronounced increase of the curve. Regarding the series resistance, the data proves the aging of the cell, since a quite high damaging is responsible for a big  $R_s$  variation. Predictably, due to the low duration of the test, the i-U curve and the power density changes are negligible, with only a small decrease in current density (4.16, c). Talking about the ASR, even in this case there is not a huge difference between this experiment and the 30% recirculation one with an increase of approximately 18% in 1000 h (see fig. 4.15, b)). As already mentioned, the high amount of tests hours performed with this cell and due to a crack, with a consequent leakage of fuel, has led to a lower voltage and, as a consequence, lower power and efficiency output than

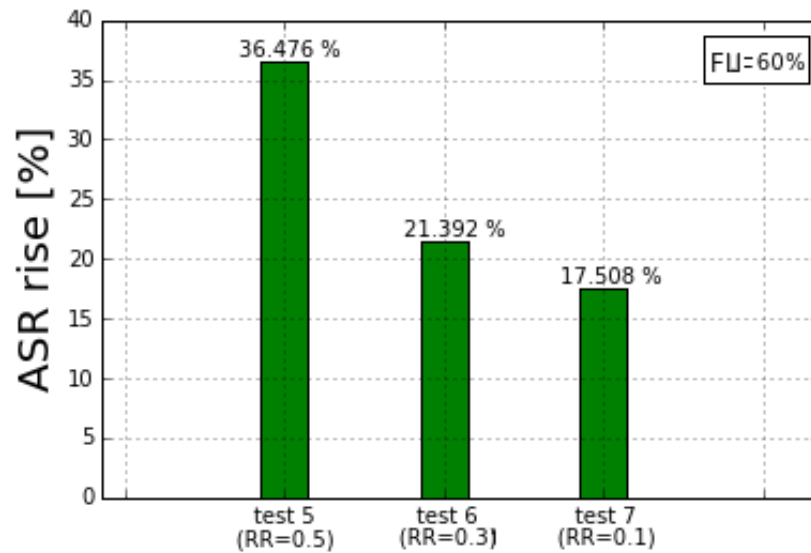
expected, but anyway better than the extra  $CO_2$  run just before starting recirculation (which was around  $0.752\text{ mV}$ ), with an increment of almost 3.5%.

Average voltage [V]	$P_{el}$ [W]	$\eta_{el}$
0.765	6.12	0.447

Table 4.16: Test 7: average voltage, power and efficiency with recirculation of 10%

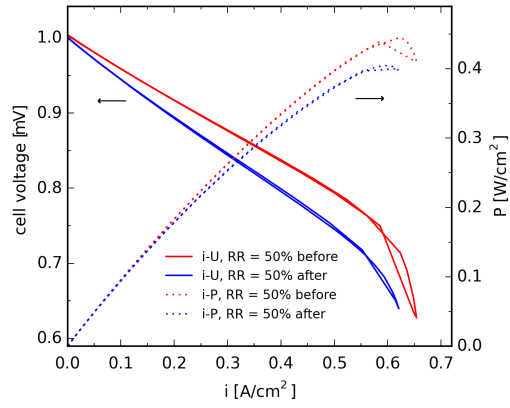


(a) Delta Bode plot for recirculation using pump applied to pre-mixed landfill biogas.

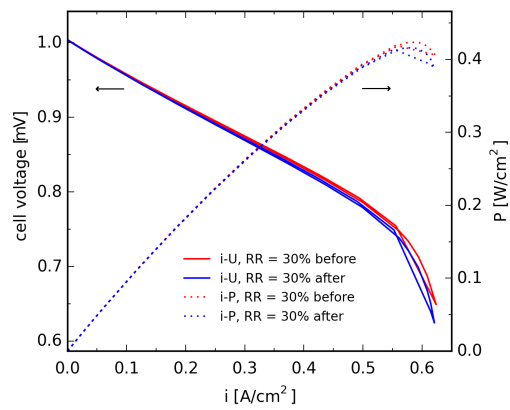


(b) ASR percentage increment in 1000 h, pre-mixed landfill.

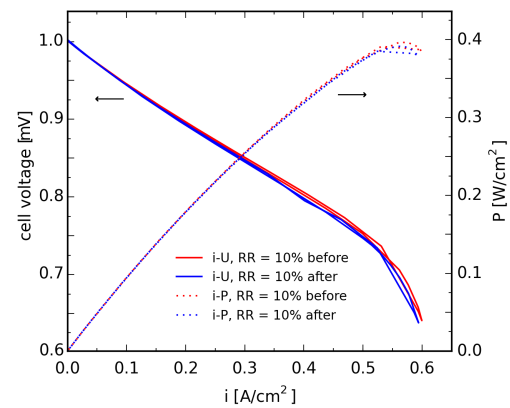
Figure 4.15: Experimental data from test 5, test 6 and test 7



(a) *i-U* curve, pre-mixed landfill  $RR = 50\%$ .

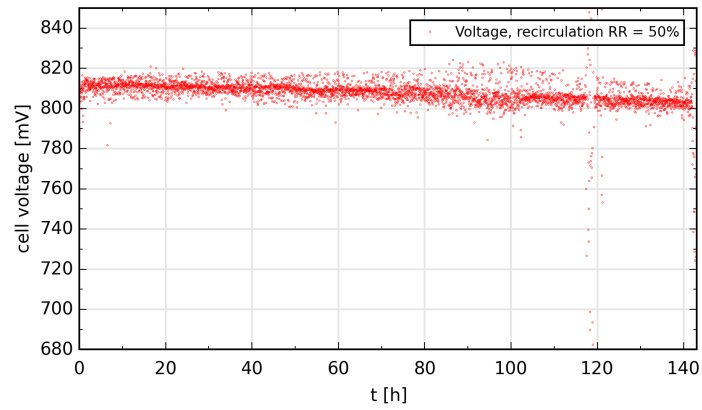


(b) *i-U* curve, pre-mixed landfill  $RR = 30\%$ .

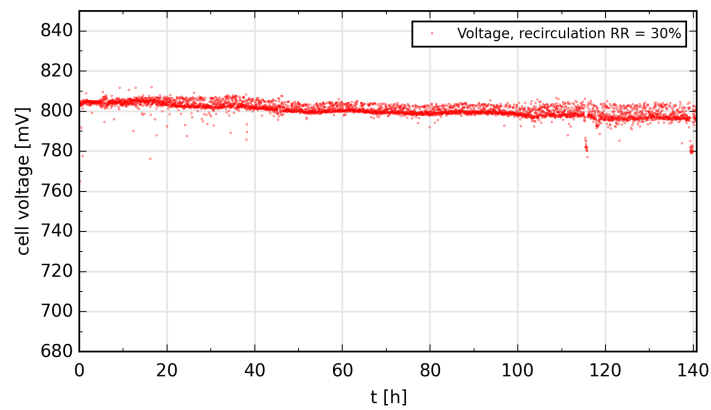


(c) *i-U* curve, pre-mixed landfill  $RR = 10\%$ .

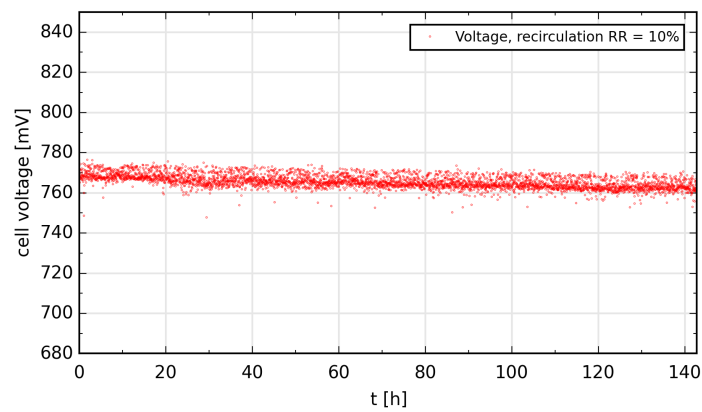
Figure 4.16: *i-U* curves from test 5, test 6 and test 7



(a) Voltage over time, pre-mixed landfill RR = 50%.



(b) Voltage over time, pre-mixed landfill RR = 30%.



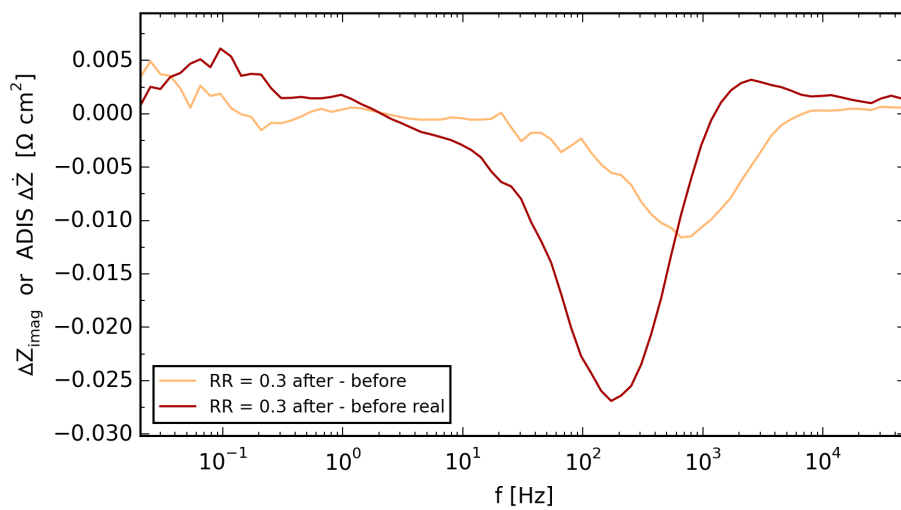
(c) Voltage over time, pre-mixed landfill RR = 10%.

Figure 4.17: Voltage evolution from test 5, test 6 and test 7

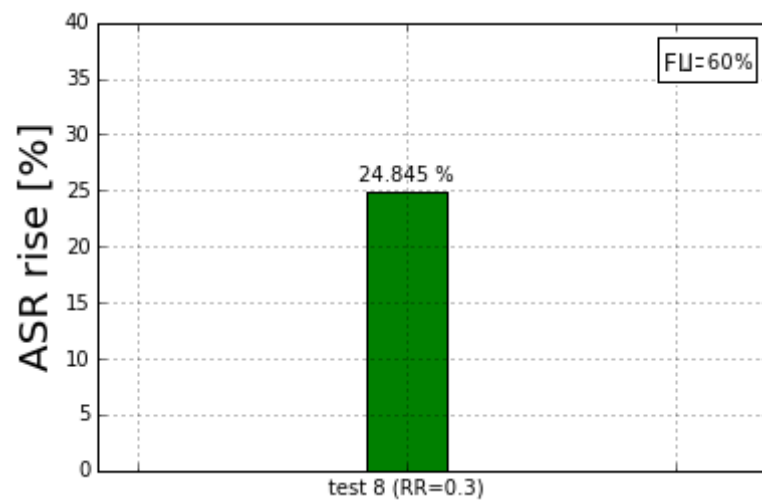
**Test 8** : In the last test performed, it has been used the real biogas, coming from Odense Renovation, repeating the experiment with a recirculation ratio of 30%, in order to have a complete overview, since this ratio has been applied to the cell in four different cases: simulation, pre-mixed biogas test with and without pump and real biogas test. Owing to the fact that this biogas contains impurities, an activated carbon filter has been adopted, able to take out especially sulphur, the most problematic compounds as already explained in section 2.2.1. Differently from the previous case, the amount of  $CH_4$ ,  $CO_2$  and  $N_2$  are not fixed, but depends on the biogas composition in the bottle, which can vary a little bit. For example, in this case the amount of methane was higher than 34%, easily recognizable by the fact that the initial voltage (tab. 4.13) is higher than expected and also looking at the i-U curve, where the maximum current density is bigger with respect to the previous cases (fig. 4.19, a)). This biogas composition variation is the reason why the test has been carried out using 30% of RR instead of the more interesting one of 10%, in order to be more sure not to have carbon deposition on the cell anode. Looking at the voltage curve (4.19, b)), the decrease is stable, but the degradation is really high (tab. 4.13), much more than test 5, in which pre-mixed biogas with the same composition has been used. As already said, the reason should be the higher amount of  $CH_4$  contained in the bottle of real biogas. The signal in the second part of the graph is fluctuating a lot due to a problem with the pump, no more able to maintain the pressure fixed. This problem could also be responsible for abnormal degradation for the cell. The trend is partially confirmed observing the evolution of the resistance polarization, which presents an increment of the degradation, passing from  $0.01 \Omega \cdot cm^2$  to  $0.02 \Omega \cdot cm^2$  (tab. 4.13), while the  $R_s$  remains almost stable. On the other hand, the behavior of the delta Bode plot is similar to test 6 (fig. 4.15, a)), with a small increase of the curve in the mass transfer zone and a high decrease in the charge transfer one: in the real biogas case, the peak is moved on the left and the maximum value is more than the double. Finally, in fig. 4.19, a) are illustrated the i-U and i-P curves, in which is possible to see a small decrement both of the current density and power density, even if as concerned the current density the value seems to be bigger due to an error of the software recorder (blue line). Moreover, that decrease is observable also in the ASR changing, reported in fig. 4.18, b), with a rise of almost 25%, which confirm the worse degradation of the cell compared to test 6. Average voltage, power and efficiency are reported in tab. 4.17: as expected, those value are lower with respect to test 6 ones, due to the fact that the cell was already quite degraded, having run for more than 2000 hours, and presenting a crack which caused a leakage, so less fuel was going inside the cell, decreasing the voltage according to Nernst (eq. 2.13).

Average voltage [V]	$P_{el}$ [W]	$\eta_{el}$
0.768	6.144	0.449

Table 4.17: Test 8: average voltage, power and efficiency with recirculation of 30%

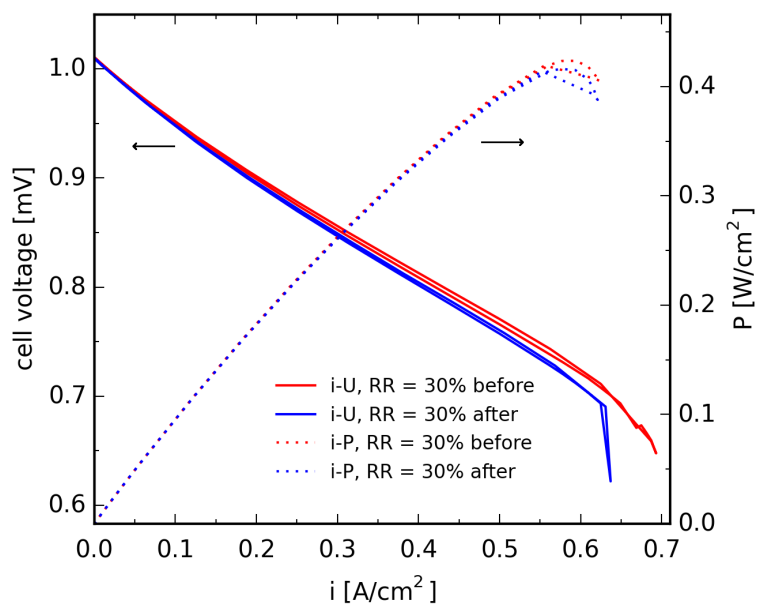


(a) Delta Bode plot for recirculation using pump applied to real biogas.

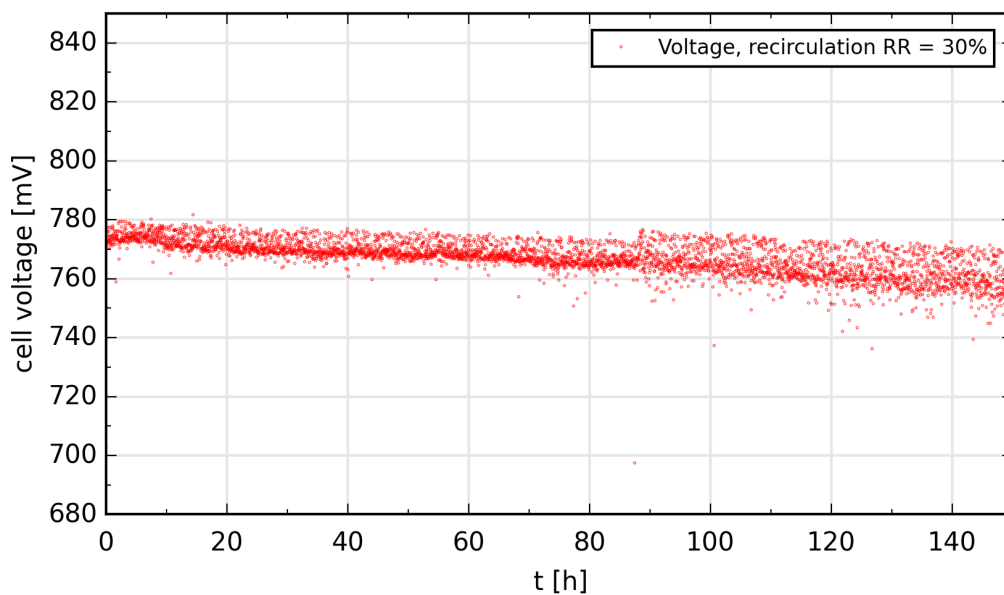


(b) ASR percentage increment in 1000 h, real biogas.

**Figure 4.18: Experimental data from test 8**



(a)  $i$ - $U$  curve, real biogas  $RR = 30\%$ .



(b) Voltage over time, real biogas  $RR = 30\%$ .

Figure 4.19: Voltage evolution and  $i$ - $U$  curve from test 8



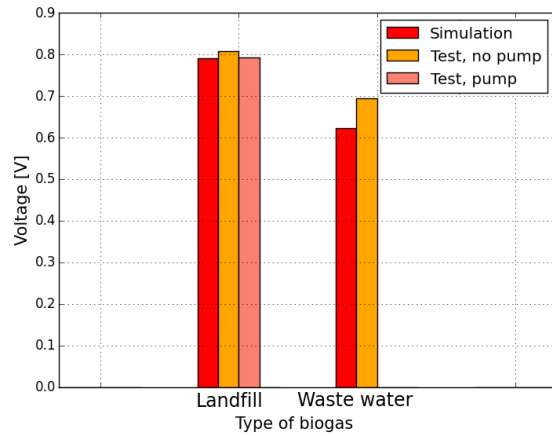
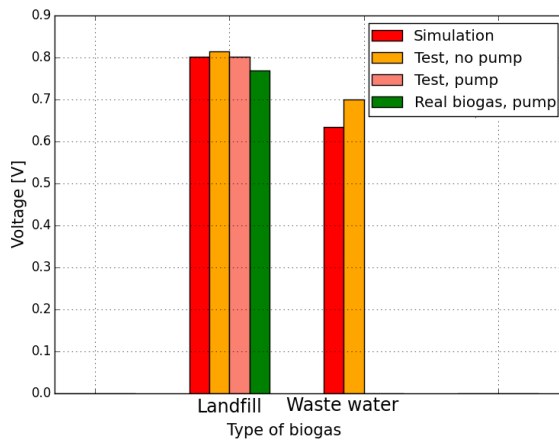
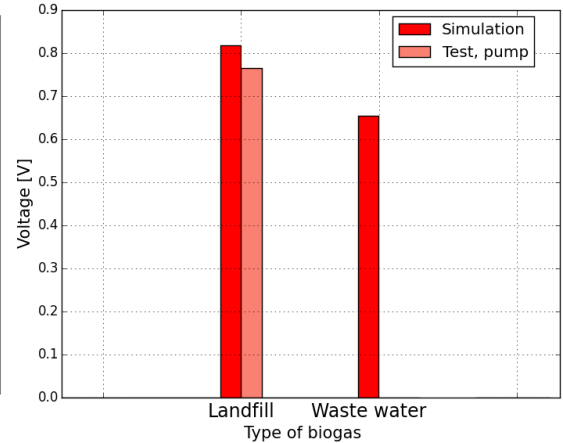
# Chapter 5

## Comparison

Finally, a comparison among the various experiments and the simulation has been done, in order to understand the behaviour of the cell under different working conditions and to prove the reliability of the simulations themselves. The first part is dedicated to the cell performance overview, including voltage and efficiency, while the second one to the degradation parameters, so  $D_r$ ,  $R_p$  and ASR.

### 5.1 Evaluation of differences in cell performance

Starting with the voltage, in fig. 5.1 are illustrated all the values, from the higher recirculation ratio to the lower one. The differences in voltage between simulations and tests are quite negligible looking at the landfill biogas, especially with a recirculation of 50% and 30%. This is not true for the last value of RR, since that test was one of the last performed in the test rig, so the cell was already degraded and present a crack, having run for approximately 2000 hours, so the value of voltage was expected to be higher than the simulation (having a crack means leakage of fuel and lower partial pressure, which affects the voltage due to Nernst, eq. 2.13). Moreover, the value obtained from the real biogas test is also lower than expected, for the same reasons of test 7. Real biogas contains also impurities, which are taken out by the carbon activated filter before entering into the cell; the filter has not a unitary efficiency, so some particles can still go inside and decreasing the performance. For the waste water biogas, the situation is a little bit different, since simulation results are much lower compared to the test one, but the deviation, which is in this case approximately 10-11%, could be caused by the overestimation of the ASR of the model, leading to such low values (due to 2.15).

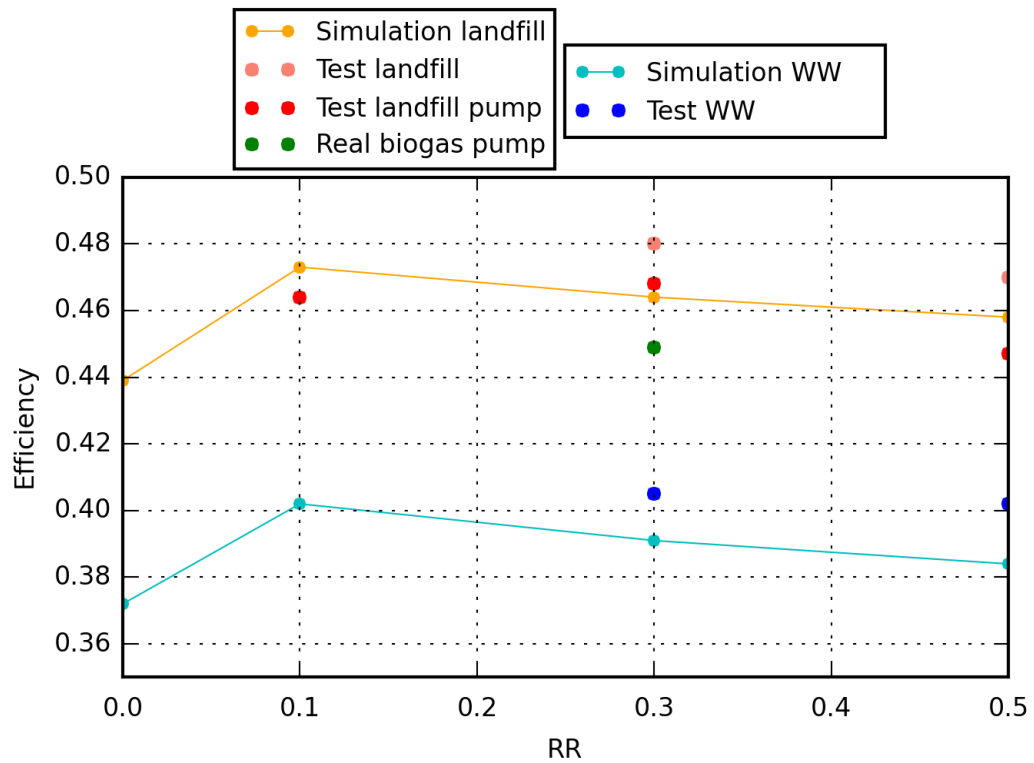
(a) Voltage,  $RR = 50\%$ .(b) Voltage,  $RR = 30\%$ .(c) Voltage,  $RR = 10\%$ .**Figure 5.1: Voltage comparison between simulations and tests**

Moving to the efficiency, a global overview has been reported in fig. 5.2, a). The two lines represent the values obtained from the simulation, while the points correspond to the experimental data. Even in this case, and especially for the landfill, the distance between points and line is not so pronounced, confirming the reliability of the simulation program. The deviation, regarding the pre-mixed recirculation, consist in 2.5% and 3.4% respectively for RR of 50% and 30%, while for the recirculation with pump, the values differ from simulation of 1.3%, 0.9% and 5.8% considering the pre-mixed biogas (respectively RR equal to 50%, 30% and 10%), and of 3.3% for the real biogas. The real biogas value is a bit more far with respect to the line, for two main reasons: the higher methane content, with respect to the pre-mixed

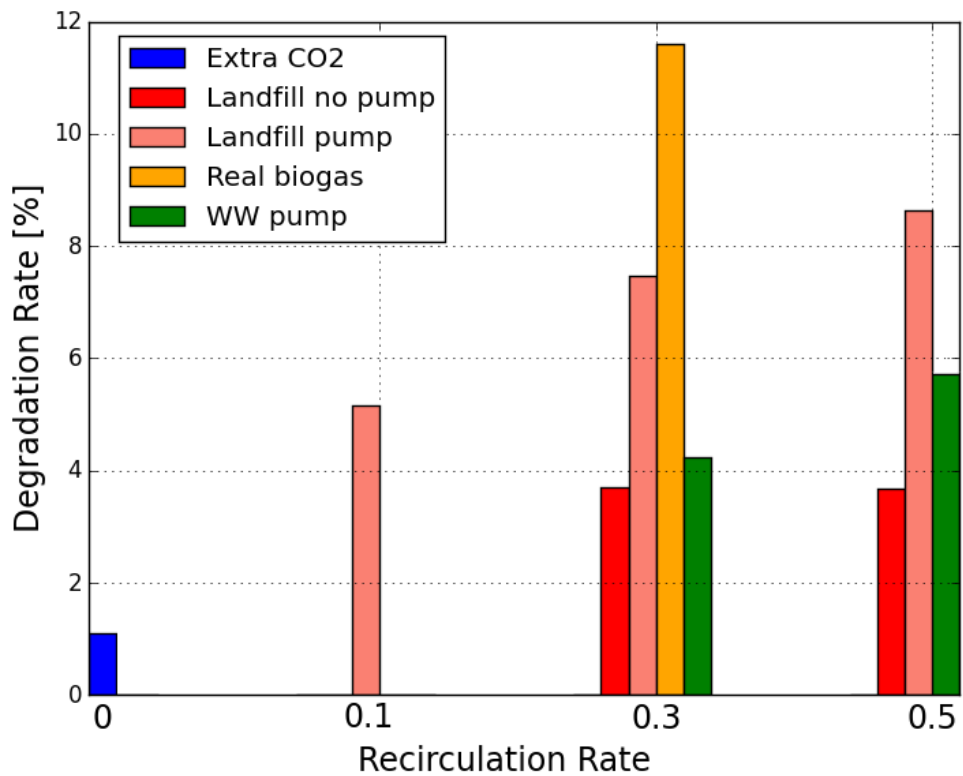
biogas, and the impurities content, which can not be completely removed by the activated carbon filter. Finally, waste water biogas presents a bigger gap with respect to landfill, in fact, the deviation results to be 11.5% and 10% for RR equal to 50% and 30%. In general, the simulations result to be underestimated in both cases.

## 5.2 Evaluation of the degradation rate for all experiments

As regards the degradation of the cell, calculated in 1000 hours, it has been evaluated for each experiment done in the rig and compared with the one obtained in no recirculation condition (test 0), so with the 2 L/h of extra  $CO_2$ . It is clear that  $D_r$  increases doing recirculation, proportionally to the RR. It also strongly depends on the biogas composition and, in particular, on the amount of methane. Everything is illustrated in fig. 5.2, b). The landfill experiments using the pump (salmon red columns) shows a decrement of approximately 2% reducing the value of RR, from 9% (RR = 50%), to 7% (RR = 30%) and finally to 5% (RR = 10%). The same trend has been shown in landfill tests 1 and 2 (red columns), in which MFCs have been used to create the recirculation: in this case, the degradation decreases with RR, but with a negligible value, difficult to capture from the graph (but numerically reported in table 4.6). For the real biogas test, degradation is really high, almost 50% more with respect to the same recirculation rate but with the pre-mixed biogas, and this effect could be caused, as already explained, by the impurities and the higher content of  $CH_4$ , but further investigations are needed to prove this hypothesis. Waste water test 3 and 4 present the same behaviour of the landfill case, but with a worse degradation, due to the amount of methane almost doubled.



(a) Simulations and tests efficiency summary.



(b) Degradation rate summary for the laboratory tests.

Figure 5.2: Efficiency and degradation rate summary

# Chapter 6

## Conclusions

The idea behind this work was to find another option to avoid carbon formation in a biogas fuelled SOFC without using a constant flow of reforming agent, trying to making use of sources already present in SOFCs. The aim, then, was not only to demonstrate that anode fuel recirculation is a valid alternative to do it, but also proving that an increase in the efficiency should occur. Therefore, simulations and experimental tests on cell level were carried out.

Applying anode fuel recirculation on SOFCs fuelled with biogas has been demonstrated to have some advantages: no external supply of reforming agent during operation is needed anymore (just for the start up and shut down extra  $CO_2$  is used), permitting to save money and space, and a not negligible gain in electric efficiency up to 4-5 percentage points has been observed. On the other hand, the degradation of the cell is higher due to the amount of water recirculated; the system results to be more complex since a pump or an ejector must be used, and therefore more expensive in the initial investment. Furthermore, it has been demonstrated that the minimum value of recirculation rate to avoid carbon deposition is proportional to the  $CH_4$  content of the biogas and to the fuel utilization since higher fuel utilization means more methane reacting inside the cell. The degradation rate is strongly dependent on RR, as the amount of steam recirculated increase with it. Finally, the efficiency is in inverse proportion to the recirculation rate, due to the fact that the lower is the recirculated flow, the lower is the inlet flow dilution and, therefore, the partial pressure of  $CH_4$  is higher and, as a consequence, the voltage, according to Nernst equation.



# Chapter 7

## Future outlook

Owing to the fact that recirculation brings with itself positive aspects:

- Savings related to the no need of external sources;
- Increasing of power output due to the higher efficiency;

but also drawbacks:

- Shorter cell lifetime due to degradation;
- Initial higher investment due to the recirculation system;

an interesting task will be the analysis of recirculation from an economic point of view. The analysis should include the evaluation of capital cost (CAPEX), which will increase due to the fact that the system is more complex, since a pump/ejector has to be included and the recirculation branch has to be developed, and operational cost (OPEX). OPEX have to be carefully evaluated, because, on the one hand, savings and efficiency rise tend to decrease operational costs, but on the other hand, the shorter lifetime of the cell leads to a more frequent substitution of it, which means higher costs. Once calculated these two costs, an estimation of the pay back time (PBT) should be performed in order to understand what is the most convenient system to implement. In addition, a further investigation to increase the cell lifetime and decrease the degradation should be done, starting from the fact that water has a key role both in degradation rise and carbon activity decrease.



# Bibliography

- [1] Spyridon Achinas, Vasileios Achinas, and Gerrit Jan Willem Euverink. “A Technological Overview of Biogas Production from Biowaste”. In: *Engineering* 3.3 (2017), pp. 299–307. ISSN: 20958099. DOI: 10.1016/J.ENG.2017.03.002. URL: <http://dx.doi.org/10.1016/J.ENG.2017.03.002>.
- [2] Nicolae Scarlat, Jean François Dallemand, and Fernando Fahl. “Biogas: Developments and perspectives in Europe”. In: *Renewable Energy* 129 (2018), pp. 457–472. ISSN: 18790682. DOI: 10.1016/j.renene.2018.03.006. URL: <https://doi.org/10.1016/j.renene.2018.03.006>.
- [3] P Lunghi, R Bove, and U Desideri. “Life-cycle-assessment of fuel-cells-based landfill-gas energy conversion technologies”. In: *Journal of Power Sources* 131.1-2 (2004), pp. 120–126. ISSN: 03787753. DOI: 10.1016/j.jpowsour.2004.01.006.
- [4] Anke Hagen, Jens F B Rasmussen, and Karl Thydén. “Durability of solid oxide fuel cells using sulfur containing fuels”. In: *Journal of Power Sources* 196.17 (2011), pp. 7271–7276. ISSN: 03787753. DOI: 10.1016/j.jpowsour.2011.02.053. URL: <http://dx.doi.org/10.1016/j.jpowsour.2011.02.053>.
- [5] A. Hagen et al. “SOFC Operation with Real Biogas”. In: *Fuel Cells* 17.6 (2017), pp. 854–861. ISSN: 16156854. DOI: 10.1002/face.201700031.
- [6] Meng Ni. “Is steam addition necessary for the landfill gas fueled solid oxide fuel cells ?” In: *International Journal of Hydrogen Energy* 38.36 (2013), pp. 16373–16386. ISSN: 0360-3199. DOI: 10.1016/j.ijhydene.2013.10.006. URL: <http://dx.doi.org/10.1016/j.ijhydene.2013.10.006>.
- [7] Hendrik Langnickel, Christopher Graves, and Anke Hagen. “Galvanostatic and potentiostatic operation of real landfill gas fueled SOFCs”. In: *13 th European SOFC & SOE Forum 2018* July (2018).

- [8] Ralph Uwe Dietrich et al. “Efficiency gain of solid oxide fuel cell systems by using anode offgas recycle - Results for a small scale propane driven unit”. In: *Journal of Power Sources* 196.17 (2011), pp. 7152–7160. ISSN: 03787753. DOI: 10.1016/j.jpowsour.2010.09.016. URL: <http://dx.doi.org/10.1016/j.jpowsour.2010.09.016>.
- [9] Joon-Ho Koh et al. “Thermodynamic Analysis of Carbon Deposition and Electrochemical Oxidation of Methane for SOFC Anodes”. In: *Electrochemical and Solid-State Letters* 4.2 (2001), A12. ISSN: 10990062. DOI: 10.1149/1.1339237. URL: <http://esl.ecsdl.org/cgi/doi/10.1149/1.1339237>.
- [10] Hendrik Langnickel. “Gibbs free energy minimization method for determining SOFC anode gas composition python program, version 1”. In: (2017).
- [11] Aline Lima da Silva and Iduvirges Lourdes Müller. “Operation of solid oxide fuel cells on glycerol fuel: A thermodynamic analysis using the Gibbs free energy minimization approach”. In: *Journal of Power Sources* 195.17 (2010), pp. 5637–5644. ISSN: 03787753. DOI: 10.1016/j.jpowsour.2010.03.066.
- [12] De Fraga Malfatti et al. “Thermodynamic analysis of ethanol steam reforming using Gibbs energy minimization method : A detailed study of the conditions of carbon deposition”. In: *International Journal of Hydrogen Energy* 34 (2009), pp. 4321–4330. DOI: 10.1016/j.ijhydene.2009.03.029.
- [13] Ryan O’Hayre, SukWon Cha, Whitney Colella, Fritz B. Prinz. *Fuel Cells Fundamentals*. Ed. by Ryan O’Hayre, Suk-Won Cha, Whitney Colella, Fritz B. Prinz. Wiley, 2016. ISBN: 9781119113805.
- [14] D.Marra. *Models for Solid Oxide Fuel Cell Systems*. Ed. by D.Marra. London: Springer-Verlag, 2016. ISBN: 9781447156574.
- [15] James Larminie and Andrew Dicks. *Fuel cell systems explained*. 2003, xxii, 406 p. ISBN: 047084857X. DOI: 10.1002/9781118878330. arXiv: arXiv:1011.1669v3. URL: <http://eu.wiley.com/WileyCDA/WileyTitle/productCd-047084857X.html>.
- [16] A. P. Baskakova; Y. V. Volkovaa; V.A. Munts; “Performance Evaluation Method of SOFC Power Unit with Anode Off-Gas Recirculation”. In: *ECS Transactions*, 78 (1) 2621-2631 (2017) 10.1149/07801.2621ecst ©The Electrochemical Society Performance 78.1 (2017), pp. 2621–2631.

- [17] E Achenbach and E Riensche. “Methane/steam reforming kinetics for solid oxide fuel cells”. In: *Journal of Power Sources* 52.2 (1994), pp. 283–288. ISSN: 03787753. DOI: 10.1016/0378-7753(94)02146-5. arXiv: arXiv:1011.1669v3.
- [18] Vincenzo Liso, Mads Pagh Nielsen, and Søren Knudsen Kær. “Influence of anodic gas recirculation on solid oxide fuel cells in a micro combined heat and power system”. In: *Sustainable Energy Technologies and Assessments* 8 (2014), pp. 99–108. ISSN: 22131388. DOI: 10.1016/j.seta.2014.08.002. URL: <http://dx.doi.org/10.1016/j.seta.2014.08.002>.
- [19] Jianjun Ma et al. “Highly efficient, coking-resistant SOFCs for energy conversion using biogas fuels”. In: *Journal of Materials Chemistry A* (2015), pp. 19068–19076. DOI: 10.1039/c5ta06421j.
- [20] Dang Saebea, Yaneeporn Patcharavorachot, and Amornchai Arpornwichanop. “Analysis of an ethanol-fuelled solid oxide fuel cell system using partial anode exhaust gas recirculation”. In: *Journal of Power Sources* 208 (2012), pp. 120–130. ISSN: 03787753. DOI: 10.1016/j.jpowsour.2012.02.023. URL: <http://dx.doi.org/10.1016/j.jpowsour.2012.02.023>.
- [21] A Hauch et al. “Sulfur Poisoning of SOFC Anodes : Effect of Overpotential on Long-Term Degradation Sulfur Poisoning of SOFC Anodes : Effect of Overpotential on Long-Term Degradation”. In: *Journal of the Electrochemical Society* (2014). DOI: 10.1149/2.080406jes.
- [22] Y Matsuzaki. “The poisoning effect of sulfur-containing impurity gas on a SOFC anode: Part I. Dependence on temperature, time, and impurity concentration”. In: *Solid State Ionics* 132.3-4 (2000), pp. 261–269. ISSN: 01672738. DOI: 10.1016/S0167-2738(00)00653-6. arXiv: 9605103 [cs]. URL: <http://linkinghub.elsevier.com/retrieve/pii/S0167273800006536>.
- [23] Fuel cells Bulletin. *Convion SOFC for DEMOSOFC project in Italy runs on biogas*. 2017. URL: <https://www.sciencedirect.com/journal/fuel-cells-bulletin>.
- [24] M Engelbracht et al. “Analysis of a Solid Oxide Fuel Cell System with Low Temperature Anode Off-Gas Recirculation”. In: *Journal of the Electrochemical Society* 162.9 (2015), F982–F987. ISSN: 0013-4651. DOI: 10.1149/2.0371509jes. URL: <http://jes.ecsdl.org/cgi/doi/10.1149/2.0371509jes>.

- [25] Chris Graves. “RAVDAV data analysis software, version 0.9.7”. In: (2012).
- [26] Anna Winiwarter. “Direct Use of Biogas in SOFCs”. In: *Master of Science Thesis* (2016).
- [27] J.- C. Njodzefon. “Electrode Kinetics and Gas Conversion in Solid Oxide Cells - DTU Findit”. In: (2015). URL: <http://findit.dtu.dk/en/catalog/2304127236>.
- [28] Andrzej Lasia. *Electrochemical Impedance Spectroscopy and its Applications*. Springer, 2014. ISBN: 9781461489320.
- [29] Rasmus Rode et al. *Solid Oxide Fuel Cell Stack Diagnostics Rasmus Rode Mosbæk Department of Energy Conversion and Storage Ph . D . Thesis , October 2014*. 2014. ISBN: 9788792986207.
- [30] Anke Hagen, Gregory B. Johnson, and Per Hjalmarsson. “Electrochemical evaluation of sulfur poisoning in a methane-fuelled solid oxide fuel cell: Effect of current density and sulfur concentration”. In: *Journal of Power Sources* 272 (2014), pp. 776–785. ISSN: 03787753. DOI: 10.1016/j.jpowsour.2014.08.125. URL: <http://dx.doi.org/10.1016/j.jpowsour.2014.08.125>.
- [31] Qiu An Huang et al. “A review of AC impedance modeling and validation in SOFC diagnosis”. In: *Electrochimica Acta* 52.28 (2007), pp. 8144–8164. ISSN: 00134686. DOI: 10.1016/j.electacta.2007.05.071. arXiv: arXiv:1011.1669v3.